3 Optical materials and waveguides

This chapter describes the substrates used in silicon photonics and the optical properties of the materials. Two typical optical waveguides are presented – strip and rib waveguides. First, we calculate the optical modes of the substrate (slab modes). Then, we consider the modes in a confined waveguide. Methods of ensuring that numerical accuracy has been achieved are presented. We also discuss optical propagation losses and the losses in 90° bends.

3.1 Silicon-on-insulator

The wafers commonly used for silicon photonics are termed "silicon-on-insulator". These are commonly used in the electronics industry for high-performance circuits. The typical 200 mm (8") wafer consists of a 725 μm silicon substrate, 2 μm of oxide (buried oxide, or BOX), and 220 nm of crystalline silicon, as shown in Figure 3.1. It is in the top crystalline silicon layer that waveguides and devices are defined. Hence, the material properties of this silicon are important for designing optical (and optoelectronic) devices.

The examples in this book are based on a top silicon thickness of 220 nm, which has been used since before 2003 (e.g. Reference [1]). The thickness is considered in Section 3.2.4. The 220 nm thickness has become a standard used in particular by multi-project wafer foundries and foundry service providers (e.g. imec, LETI, IME, see also Section 1.5.5). However, it should be noted that other thicknesses are also in use (e.g. Luxtera, Kotura, Skorpios). It should be noted that the optimum thickness is application dependent and that 220 nm may not be the optimal choice [2].

The thickness variation of the top silicon is also an important parameter, and can have a variation range of +/− 5 nm (see References [3, 4] and Section 11.1 for discussions on non-uniformity). The material is typically intrinsic, with a light doping density of 1×10^{15} cm^{-3}.

3.1.1 Silicon

In this section, we describe silicon's refractive index wavelength and temperature dependence. The effect of free carriers is considered in Section 6.1.1.

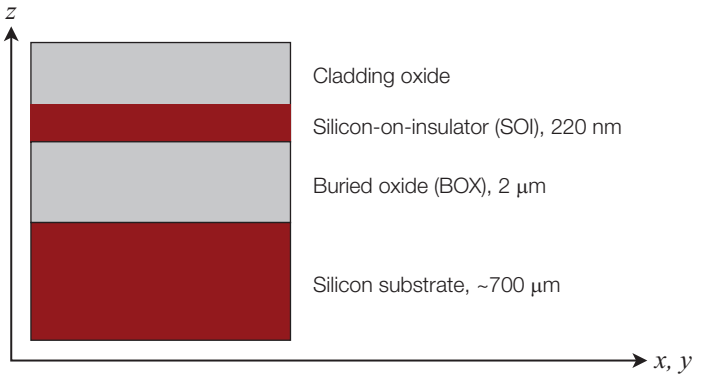

Figure 3.1 Cross-sectional view of silicon-on-insulator (SOI) wafer.

Silicon – wavelength dependence

We are interested in designing devices for a variety of wavelengths, hence the refractive index wavelength dependence of silicon and silicon dioxide should be taken into account in order to correctly describe the dispersion effects. The simplest model for silicon's wavelength dependence is a first-order dependence of -7.6×10^{-5} nm^{-1} [5]. For a more complete description, the Sellmeier equation is typically used to describe the index of refraction of materials:

$$n^2(\lambda) = \epsilon + \frac{A}{\lambda^2} + \frac{B\lambda_1^2}{\lambda^2 - \lambda_1^2}. \tag{3.1}$$

However, this model cannot be used directly for FDTD simulations. Instead, a Lorentz model [6] can be used:

$$n^2(\lambda) = \epsilon + \frac{\epsilon_{\text{Lorentz}}\omega_0^2}{\omega_0^2 - 2i\delta_0 2\pi c/\lambda - \left(\frac{2\pi c}{\lambda}\right)^2}. \tag{3.2}$$

The advantage of using this model is that the same material model for silicon in both eigenmode (Section 2.1) and FDTD calculations (Section 2.2.1) can be used to ensure consistent simulations. Appropriate coefficients are chosen to match the silicon data (from Palik's handbook [5]) over a wavelength range of 1.15 to 1.8 μm: $\epsilon = 7.9874$, $\epsilon_{\text{Lorentz}} = 3.6880$, $\omega_0 = 3.9328 \times 10^{15}$, $\delta_0 = 0$. This model satisfies Kramers–Kronig relations hence is compatible with FDTD modelling. It is also lossless for $\delta_0 \to 0$. A plot of the experimental data and Equation (3.2) is shown in Figure 3.2. Implementation of the material in a Lumerical script is provided in Listing 3.1.

Silicon – temperature dependence

The modification of the refractive index in silicon is due to the changes in the distribution functions of carriers and phonons, and the temperature-induced shrinkage of the bandgap [7]. As we will see, a slight modification of the temperature will shift the transmission spectrum of photonic devices such as ring resonators. This will be useful for thermally tuning devices.

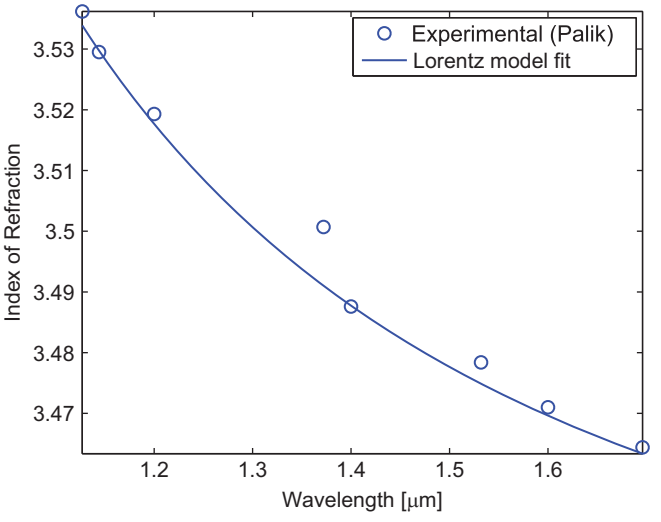

Figure 3.2 Index of refraction of silicon at room temperature, $T = 300$ K. Data fit using Lorentz model.

The temperature dependence can be approximated as $\beta = \frac{1}{n}\frac{dn}{dT}$, which for silicon is 5.2×10^{-5} K^{-1} [8–10]. It has also been measured to be $\frac{dn}{dT} = 1.87 \times 10^{-4}$ K^{-1} at 1500 nm [11].

3.1.2 Silicon dioxide

Silicon dioxide, SiO_2 (also termed glass, or silica), has a nearly constant index of refraction around 1.444 at 1550 nm (material dispersion is about 6× lower than in silicon, i.e. -1.2×10^{-5} nm^{-1}). Silicon dioxide's temperature dependence is also 6.3× lower than silicon [10]. In addition, most of the light is confined in the silicon, hence the oxide dispersion and temperature dependence does not play a significant role in the performance of silicon photonic circuits. The inclusion of the oxide dispersion may be important for waveguides where light is present outside the waveguide, e.g. in slot waveguides, or in thin waveguides. In such a case, the model presented in Figure 3.3 can be used. Implementation of the material in a Lumerical script is provided in Listing 3.1.

However, for FDTD simulations, it is often preferable to choose a simpler model (fewer convergence issues, faster simulation time), specifically the constant index model ($n = 1.444$ at 1550 nm). The error introduced by using a constant index versus the dispersive one, for the group index of a 500 × 220 nm strip waveguide, is about 0.1%. Hence, we generally use the constant index model in FDTD and MODE simulations.

3.2 Waveguides

There are several types of waveguides used in silicon photonics. The strip waveguide (also known as channel, photonic wire, or ridge waveguide), Figure 3.4(left), is typically

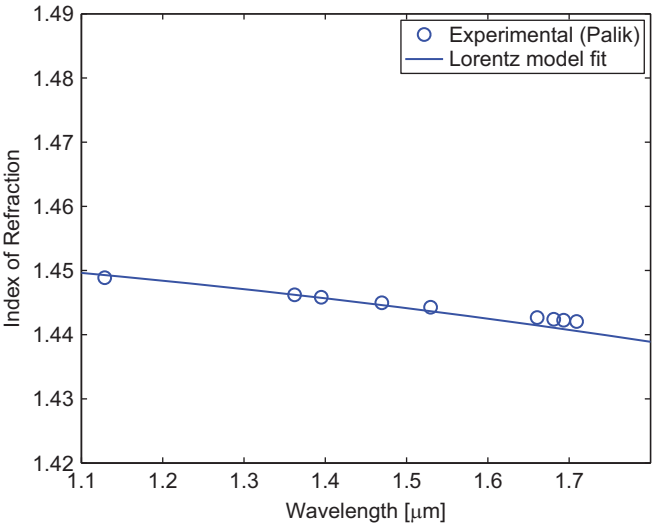

Figure 3.3 Index of refraction of silicon dioxide (SiO_2) at room temperature, $T = 300$ K. Data fit using Lorentz model.

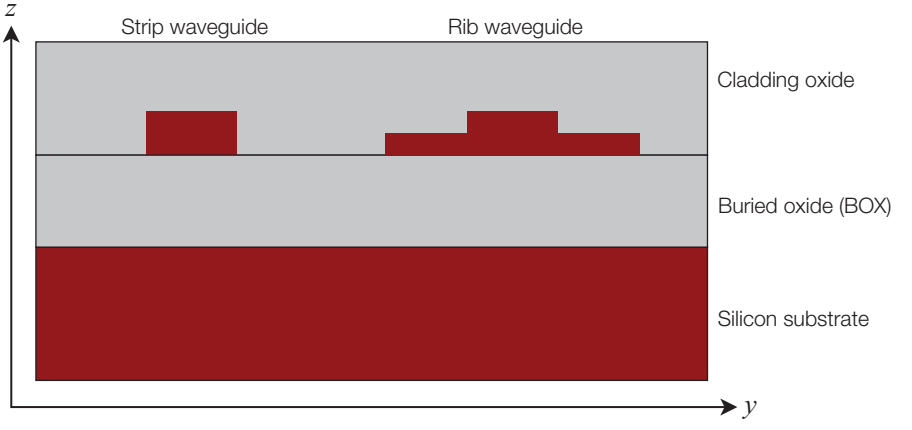

Figure 3.4 Common waveguides in silicon photonics. (Left) Strip waveguide, also known as channel waveguides, photonic wires, or ridge waveguides. (Right) Rib waveguide, also known as ridge waveguide or strip-loaded ridge waveguide.

used for routing as it offers tight bend radii. The rib waveguide (also known as strip-loaded ridge, or ridge waveguide), Figure 3.4(right), is used for electo-optic devices such as modulators, since it allows for electrical connections to be made to the waveguide. Both waveguides can be made to have a loss of less than 3 dB/cm.

Oxide cladding is used to protect the devices and to permit the fabrication of metal interconnects above the waveguides. Waveguides can also be fabricated without the cladding, for example, for evanescent field sensors for lab-on-chip applications [12–14].

3.2.1 Waveguide design

Waveguide design typically has the following procedure.

- First, one-dimensional (1D) calculations are performed to determine the slab waveguide modes, as supported by the wafer (with appropriate coating, e.g. oxide) as in Figure 3.1. This can be done analytically (Section 3.2.2) or numerically (Section 3.2.3). The silicon thickness is chosen based on requirements, e.g. supports only a single TE and TM waveguide mode. The thickness is typically constrained to what is available by the foundry, e.g. SOI thickness of 220 nm, or etched silicon with a 90 nm thickness.
- For the given thickness, find a suitable waveguide width, again, to meet requirements, e.g. supports only a single TE and TM waveguide mode. This can be done using the effective index method (EIM, Section 3.2.5), or a fully vectorial 2D method (Section 3.2.7).
- Additional consideration should be given to waveguide bend loss, substrate leakage, etc.

The simulations described next, in Sections 3.2.2–3.2.10, are focused on waveguide properties including the effective index, mode profile, and the group index in Section 3.2.9.

3.2.2 1D slab waveguide – analytic method

The MATLAB code in Listing 3.2 finds the effective index of the slab waveguide for the TE and TM modes. For the example we are considering in this section, the command is invoked using:

```
[n_te, n_tm] = wg_1D_analytic (1.55e-6, 0.22e-6, 1.444, 3.473, 1.444)
```

The effective index is found to be 2.845 for the TE mode, and 2.051 for the TM mode. Note that this example solves the waveguide at a single wavelength. To perform wavelength sweeps, the material dispersion should be included. Mode profiles can also be calculated, using MATLAB Script 3.3.

This technique is also used for the design of fibre grating couplers, in Section 5.2.

3.2.3 Numerical modelling of waveguides

In this section, we model the waveguide using a numerical eigenmode solver. First, the waveguide geometry is drawn. The code in Listing 3.4 creates the structure for the wafer and the waveguides, in Lumerical MODE Solutions, as in Figures 3.4 and 3.5. It is then solved as a slab waveguide (1D), then using the effective index method, and finally the fully vectorial 2D solution for the waveguide cross-section (2D). We use the material models defined in Listing 3.1.

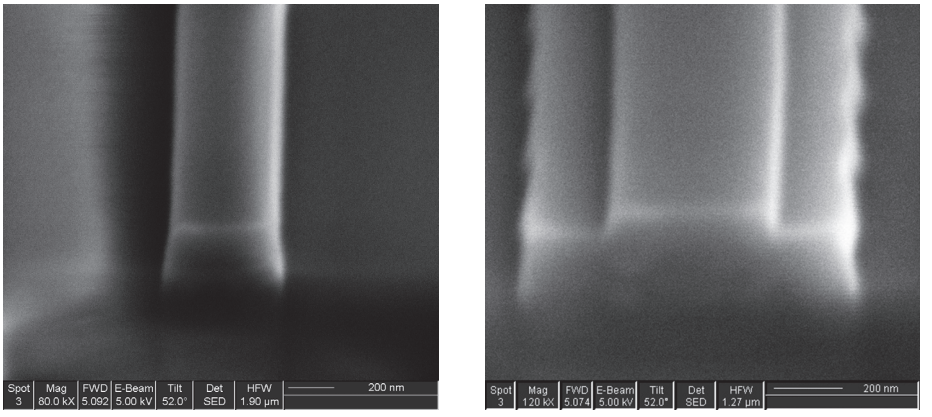

(a) Strip waveguide (b) Rib waveguide

Figure 3.5 SEM cross-sectional images of strip and rib waveguides. Note: the rib waveguide has intentional corrugations used to fabricate Bragg gratings (see Section 4.5). Reference [15].

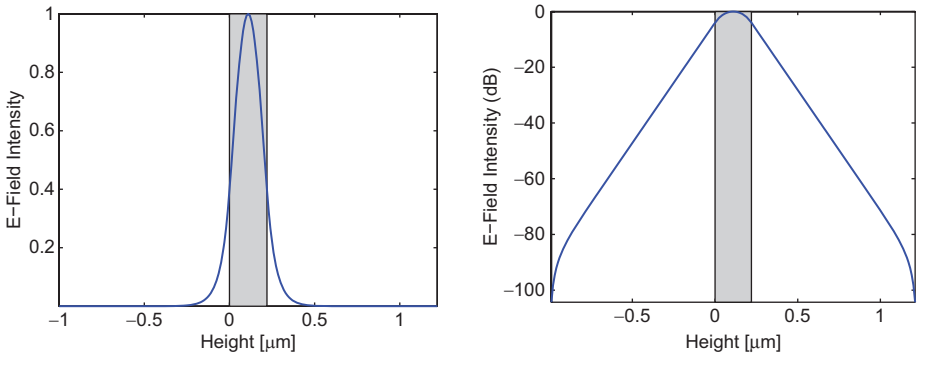

(a) Linear scale (b) Log scale, dB

Figure 3.6 The fundamental mode profile of the slab waveguide (TE). The effective index of this mode is 2.845. Calculated using the eigenmode solver. The waveguide dimension is indicated by the grey area.

3.2.4 1D slab – numerical

First, we simulate the slab waveguide modes, of the structure in Figure 3.1. The first step is configuring a 1D eigenmode solver in the cross-section of the waveguide. This is done in Script 3.5. Next, the calculation is performed in Listing 3.6 and modes profiles are plotted.

The first two modes of the slab waveguide are shown in Figure 3.6 (TE polarization) and Figure 3.7 (TM polarization). This geometry supports only two modes at 1550 nm. The log-scale plots are useful to ensure that the field profile has decayed sufficiently so that the simulation boundaries do not affect the results. The figures also show that the field profiles decay at different rates, namely the TE mode has a stronger confinement. In general, higher effective index modes are more tightly confined to the waveguide

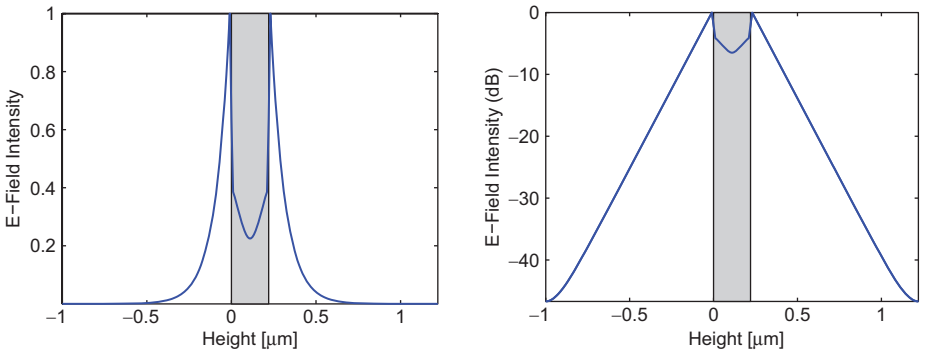

(a) Linear scale (b) Log scale, dB

Figure 3.7 The mode profile of the 2nd mode in the slab waveguide (TM). The effective index of this mode is 2.054. Calculated using the eigenmode solver. The waveguide dimension is indicated by the grey area.

and have more rapidly decaying evanescent tails. The decay of the field profile in the cladding can be approximated by:

$$E \propto e^{-\frac{2\pi d}{\lambda}\sqrt{n_{\text{eff}}^2 - n_c^2}}, \tag{3.3}$$

where E is the field amplitude at a distance, d, from the core–cladding interface, n_{eff} is the effective index of the mode, and n_c is the refractive index of the cladding.

Convergence tests

When doing numerical simulations, it is critical to do convergence tests. This ensures that the simulation is free from numerical artifacts. In the following example, we will ensure that the simulation boundaries do not interfere with the simulation results. It is easiest to perform convergence tests by ensuring that only one parameter in the simulation is changing; for example, the mesh points inside the waveguides should remain at the same positions during a parameter sweep for the simulation span, as discussed next.

Script 3.7 calculates the effective index versus the simulation span, with results shown in Figure 3.8a. The TE mode is calculated by selecting mode #1, and the TM mode is calculated by selecting mode #2. For the TE mode, simulation spans of larger than 1300 nm converge to an effective index variation of less than 0.0001. This suggests that 550 nm above and below the waveguide is sufficient for accurate simulations of TE modes. We will use this information for optimizing the 3D FDTD simulations. We can compare this span to the results in Figure 3.6 to determine that the E-field intensity should decay down to 10^{-6} of its maximum value to ensure that the boundary does not perturb the mode. Because the TM field profile has a larger tail (this can be inferred from the lower effective index), the simulation converges at larger spans, hence this mode requires a larger simulation volume for accurate modelling. In this case, the TM mode requires spans of 2000 nm for the same precision. Figure 3.8b plots the absolute error in terms of the difference in effective index (compared to the 2000 nm result). The

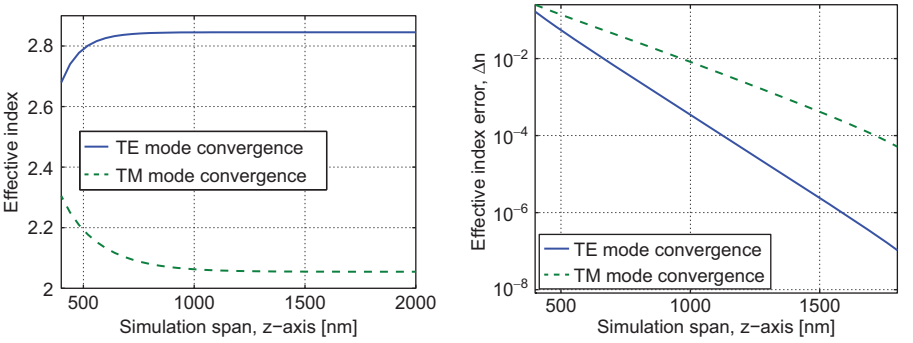

(a) TE & TM mode effective index

(b) Error in effective index; log scale

Figure 3.8 Convergence tests for slab mode calculations (varying the simulation size).

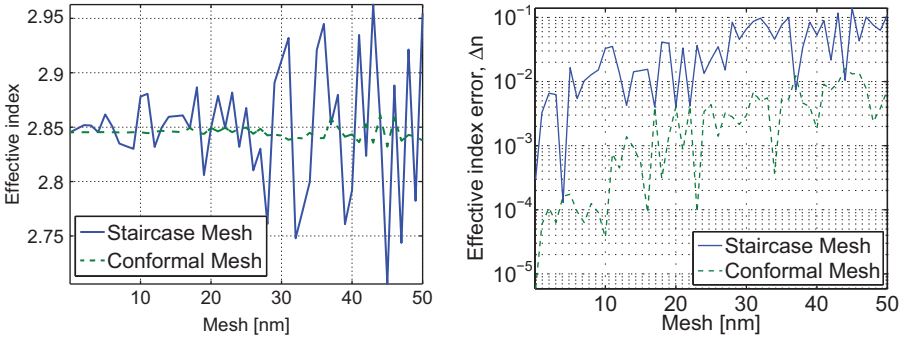

(a) Effective index vs. mesh size

(b) Error in effective index

Figure 3.9 Convergence tests for slab mode calculations (varying the mesh grid), for the TE mode.

error is exponentially reduced for increasing simulation size, where a $\Delta n = 10^{-6}$ error is found for a span of 1600 nm.

Next, we study the impact of the mesh grid on the precision. In this case, we set the simulation span to be large, 2 μm in this case, and plot the results for the TE mode. Conventional algorithms use a staircase mesh, which introduces significant error unless the mesh is reduced down to 1 nm or smaller (which is typically not practical as it results in long simulation times), as shown in Figure 3.9a(staircase) and Figure 3.9b(staircase). For a typical mesh size of 10 nm, the staircase mesh introduces an error of $\delta n_{\text{eff}} = 0.05$. To improve the accuracy, mesh overrides can be used to increase the number of mesh grid points in areas of interest. It is also advisable to have a grid point lie at each material interface.

Advanced algorithms, such as the conformal mesh, improve the accuracy significantly. In fact, a 20 nm conformal mesh has a similar accuracy as the 1 nm staircase mesh. Using the conformal mesh, from Figure 3.9b(conformal), we find that a mesh of 10 nm results in an error of approximately $\Delta n = 10^{-4}$, and a mesh of 20 nm results

in an error of approximately $\Delta n = 10^{-3}$. Even for large meshes such as 40–50 nm, the error is typically less than $\Delta n = 10^{-2}$.

These simulations are implemented in Script 3.8. The meshing algorithm is selected using the "mesh refinement" parameter.

Parameter sweep – slab thickness

Next, we wish to study the effective index of the slab versus the slab thickness. Script 3.9 performs the simulation sweep with results shown in Figure 3.10. The effective index as well as the polarization fraction (TE vs. TM) is returned. Note that, for a 1D waveguide structure, the mode is either a pure TE or a pure TM mode. This is in contrast to the 2D waveguides, where pure TE or TM modes do not exist. The TE/TM polarization fraction is used to label the modes in Figure 3.10. The dotted line is the index of refraction of the oxide; modes with index below this value are not guided.

As can be seen, at a wavelength of 1550 nm, the slab operates in a single TE and TM mode for thicknesses below 240 nm (indicated by the vertical line, which shows the onset of guiding for the third mode). This explains why 220 nm is commonly chosen for silicon-on-insulator substrates for a wavelength of 1550 nm. These graphs are useful in designing waveguides with different thicknesses, wavelengths, and polarization.

3.2.5 Effective Index Method

To calculate the effective index of a 2D waveguide cross-section, as in Figure 3.4, the Effective Index Method can be used (see Section 2.2.3). Although fully vectorial 2D solutions are more accurate (Section 3.2.7), this method provides important insights into how waveguides operate. Also, this method is computationally very fast and easy to implement, hence is used for designing modulators in Section 6.2.2, and for 2.5D FDTD simulations (Section 2.2.3).

To calculate the TE-like modes, we first find the 1D slab out-of-plane TE mode (this defines that it is predominantly a TE mode), and then we find the 1D in-plane TM mode using the effective index from the 1D slab. The change of polarization is necessary since we are solving a 2D problem using two 1D simulations; hence we are rotating the frame of reference with respect to the primary field component (e.g. in-plane E-field for the TE-like mode). For TM-like modes, the reverse procedure is used: first the TM mode for the slab, followed by the TE mode.

As an example, to find the TE-like mode, first, the slab effective index is found, for the out-of-plane cross-section, as per Listing 3.6. The procedure is repeated, except this time in the in-plane direction. The slab effective index is used as the input into this second step. The final result is the effective index of the 2D waveguide. The script in Listing 3.10 accomplishes this, where we have used the slab TE mode effective index (2.845) as the input, with the aim of calculating the TE mode effective index of the strip waveguide. The result is a waveguide effective index of 2.489 with a field profile as shown in Figure 3.11.

Using the mode profiles in Figure 3.6a and Figure 3.11a, we can construct the 2D mode profile. The inherent assumption in the Effective Index Method is that the fields

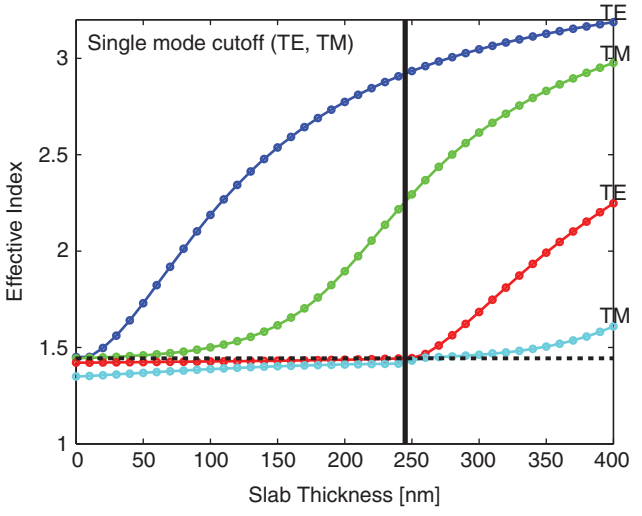

(a) Wavelength of 1550 nm.

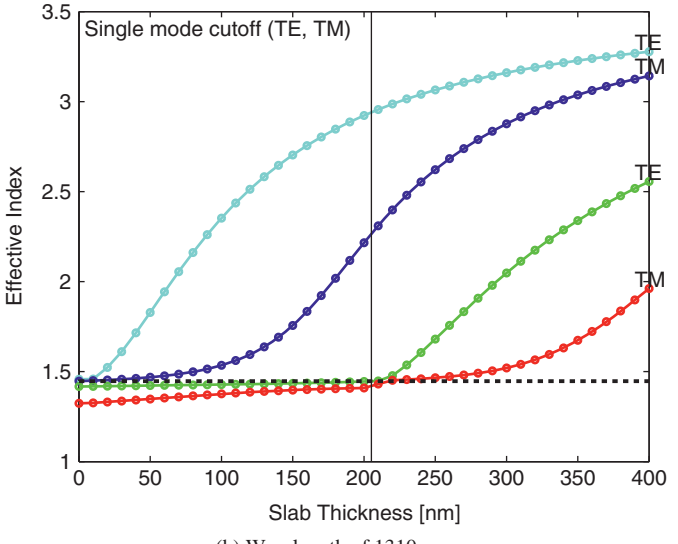

(b) Wavelength of 1310 nm.

Figure 3.10 Simulation of the effective index of the slab waveguide modes versus the thickness of silicon. Waveguide is cladded with silicon dioxide. Only the modes above the dotted lines are guided.

are separable, similar to the method of "separation of variables" for solving differential equations. Here, we write the 2D field profile as

$$E(z, y) = E(z) \cdot E(y),$$

where $E(z)$ and $E(y)$ refer to the fields in Figure 3.6a and Figure 3.11a, respectively. The resulting mode profile $E(z, y)$ is plotted in Figure 3.12a. We compare the mode profile determined by the Effective Index Method with the "exact" 2D finite element

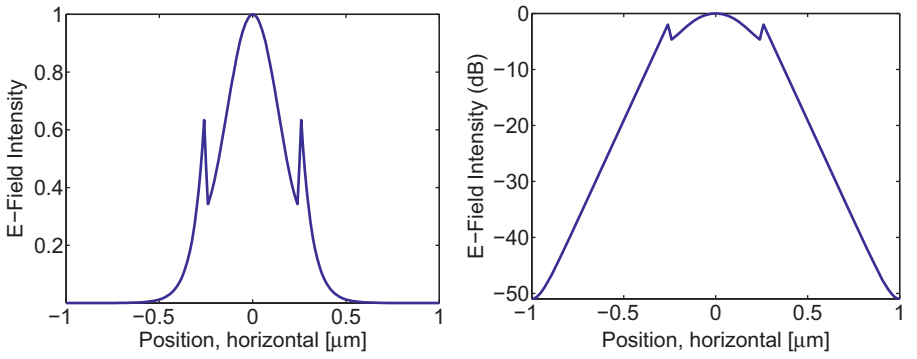

(a) Linear scale (b) Log scale, dB

Figure 3.11 The fundamental mode profile of the waveguide (TE), using Effective Index Method (EIM). The effective index of this mode is 2.489.

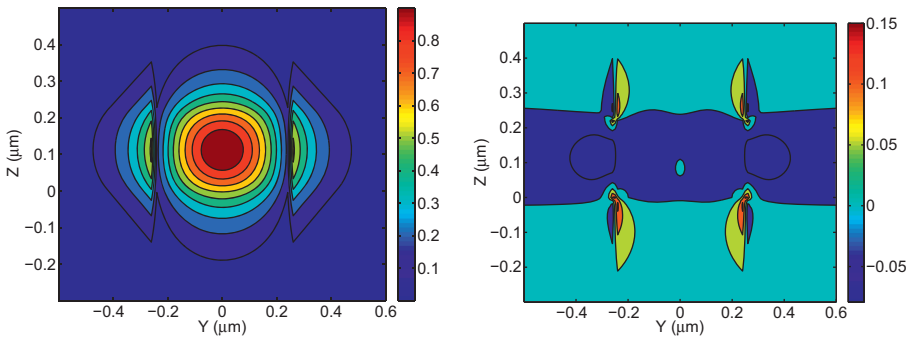

(a) Effective Index Method (b) Error in mode profile due to Effective Index Method

Figure 3.12 Comparison of the Effective Index Method reconstructed field profile versus the 2D fully vectorial calculation for a strip waveguide.

calculations in Section 3.2.7, by taking the difference of the mode profiles, with results shown in Figure 3.12b. The error in effective and group index are $\Delta n_{\text{eff}} \sim 1.2\%$ and $\Delta n_g \sim 2.7\%$ for the strip waveguide considered.

This result is useful in that we can use the Effective Index Method in combination with 2D FDTD modelling (2.5D FDTD, see Section 2.2.3), and anticipate an error in the group index of only several percent. This translates into a several percent error in the free-spectral range in resonators, but with dramatically reduced computation time as compared with full 3D simulations, which is useful when performing numerous simulations for optimization.

3.2.6 Effective Index Method – analytic

Similarly, we can use the analytic method to find the 1D field profiles (MATLAB code 3.3) and construct the 2D field profile using the Effective Index Method. This

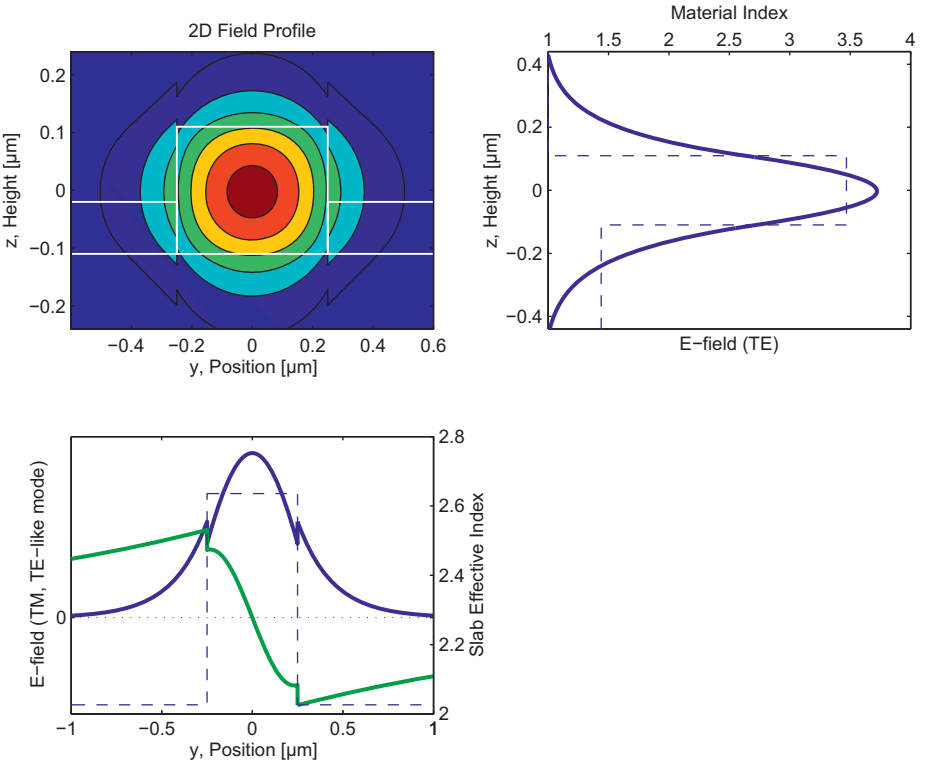

Figure 3.13 Analytic calculation of 2D waveguide field profile for a rib waveguide using the Effective Index Method, in MATLAB. (Top left) Rib waveguide geometry, with the resulting 2D field profile calculated by the Effective Index Method for the fundamental mode. (Top right) Material index of refraction for the air–silicon-oxide silicon-on-insulator wafer (shown in the dashed line), and the calculated 1D field profile in the vertical cross-section of the 220 nm waveguide; this procedure is also repeated for the slab regions (90 nm). (Bottom left) Slab effective indices calculated from step 1 (shown in the dashed line); 1D field profiles in the horizontal cross-section of the waveguide for the two guided TE-like modes.

implemented in the MATLAB code 3.11, with the results for a rib waveguide shown in Figure 3.13. This is used for modelling pn-junction modulators in Section 6.2.2.

3.2.7 Waveguide mode profiles – 2D calculations

Next, we wish to perform accurate calculations for the mode profile for the 2D cross-section of the waveguide. In this section, we draw the waveguide, define the simulation parameters, and solve for the mode solution using the fully vectorial method described in Section 2.1. We wish to find the mode profiles for quasi-TE and quasi-TM modes, and observe the electric field intensity, magnetic field intensity, and the energy density, as shown in Figures 3.14–3.17. The three field components in the x, y, and z directions are shown in Figure 3.15; from the figure, it is evident that the mode is not strictly a TE

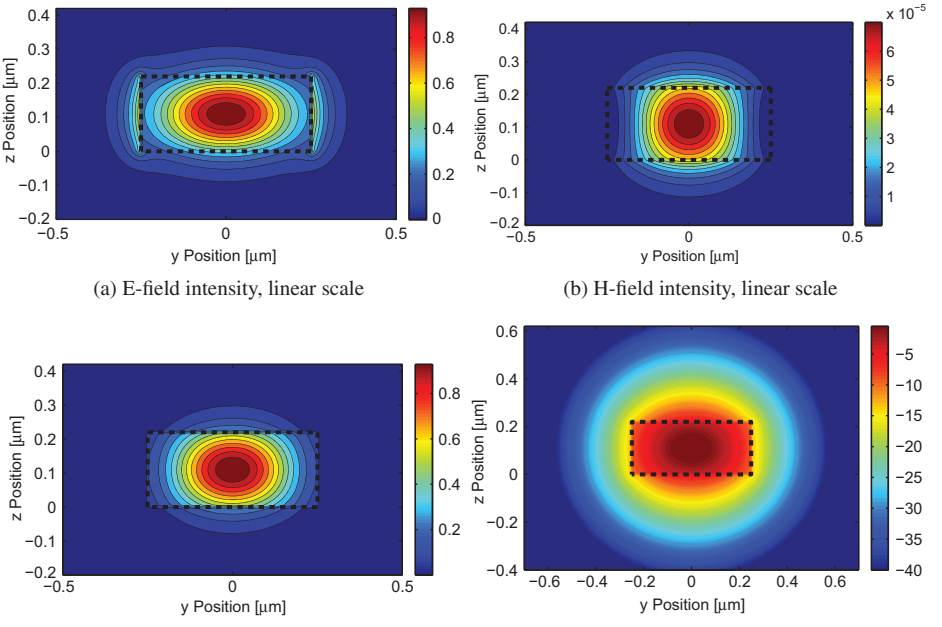

(a) E-field intensity, linear scale

(b) H-field intensity, linear scale

(c) Energy density, linear scale

(d) Energy density, log scale, dB

Figure 3.14 TE (first mode) mode profile of a 500 × 220 nm strip waveguide at 1550 nm, mode effective index is $n_{\text{eff}} = 2.443$.

mode (where only the E_y component would be present), but rather is a three-dimensional vectorial field profile.

We continue the Lumerical script by using the materials (Script 3.1) and waveguide (Script 3.4) previously described. First, we define the simulation parameters and add a 2D mode solver in the cross-section of the waveguide, in Listing 3.12. Next, in Script 3.13, we calculate the mode profiles and plot the E-field and H-field intensities, as well as the energy densities. The energy density plot requires the waveguide dispersion, hence the script calculates the mode effective index at two slightly detuned frequencies, see Reference [16].

Figures 3.14–3.17 show the results of the first three modes supported by the waveguide. Figure 3.14 shows the fundamental mode profile, in this case, with a TE-like polarization. The field and energy is strongly confined inside the waveguide, although about 10% of the field is in the cladding. This is the mode used for most silicon photonics devices for the 220 nm thickness SOI wafer.

Figure 3.16 shows the TM-like mode. This mode is well-enough confined to be useful for TM-like mode devices. However, some researchers have used a slightly thicker silicon, e.g. 260 nm [17, 18], for applications specifically targeting TM-like mode operation.

Finally, Figure 3.17 shows the TE-like mode. The effective index of the mode is close to that of the oxide, and there is a significant E-field on the edges of the waveguide. This will introduce a significant scattering loss, hence this mode will experience a high

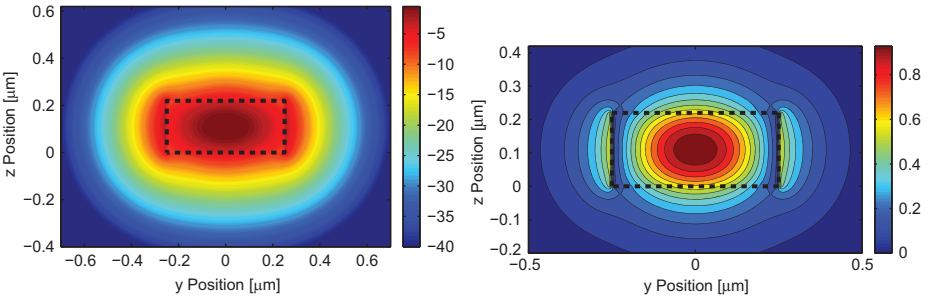

(a) E-field intensity, $|E_x|^2 + |E_y|^2 + |E_z|^2$, log scale

(b) $Re(E_y)$, linear scale

(c) $Re(E_z)$, linear scale

(d) $Im(E_x)$, linear scale

Figure 3.15 TE (first mode) mode profile of a 500 × 220 nm strip waveguide at 1550 nm. The three field components in the x, y, and z directions are shown.

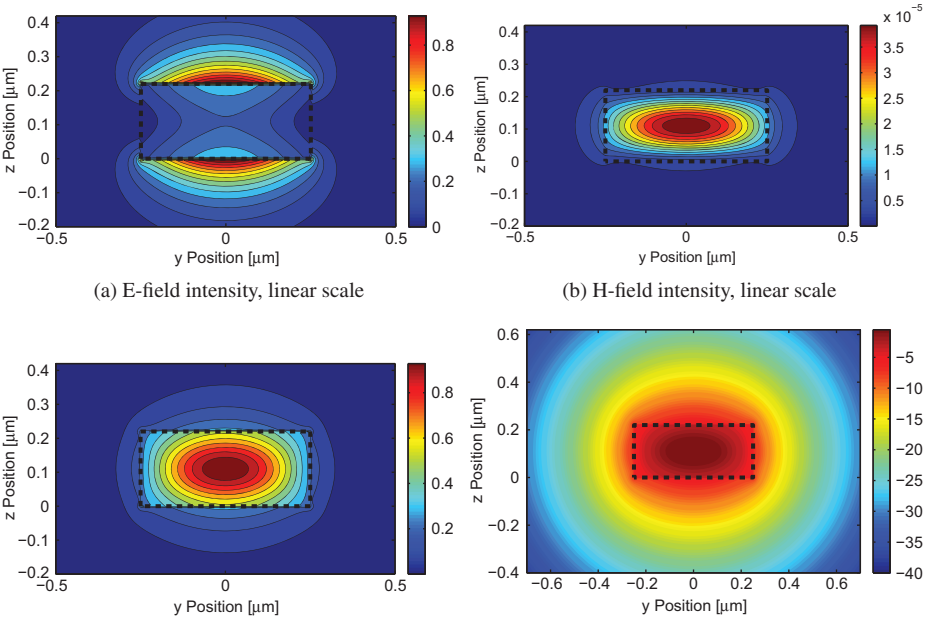

(a) E-field intensity, linear scale

(b) H-field intensity, linear scale

(c) Energy density, linear scale

(d) Energy density, log scale, dB

Figure 3.16 TM (second mode) mode profile of a 500 × 220 nm strip waveguide at 1550 nm, mode effective index is $n_{\text{eff}} = 1.771$.

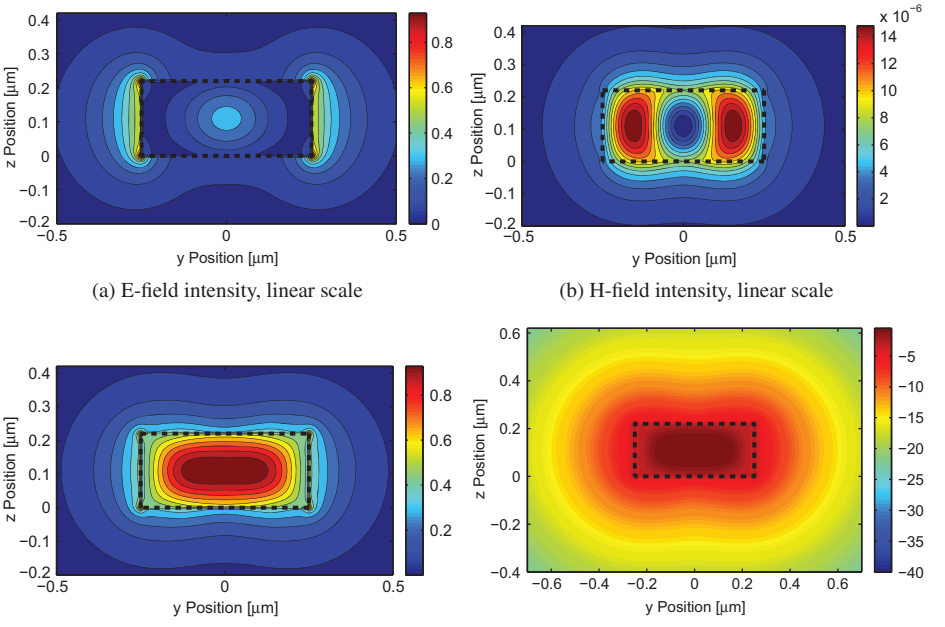

Figure 3.17 TE (third mode) mode profile of a 500 × 220 nm strip waveguide at 1550 nm, mode effective index is $n_{\text{eff}} = 1.493$. This mode is barely guided and the effective index is close to the oxide index. It will experience high optical loss due to strong side-wall scattering.

level of loss. Thus, this waveguide geometry can be considered to effectively operate as a single TE-like mode waveguide. If more mode selectivity is required, a narrower waveguide can be chosen, e.g. 440 nm, as will be found in the next section.

3.2.8 Waveguide width – effective index

Next, we vary the width of the waveguide (from 200 nm to 800 nm), in Listing 3.14, using fully vectorial 2D mode calculations. This allows us to determine the single-mode condition for the waveguide. The effective index of all modes is saved in a matrix, n_{eff}, and plotted.

The results are shown in Figure 3.18a for 1550 nm, and Figure 3.18b for 1310 nm.

For 1550 nm, only the modes above the dotted lines are guided. To obtain a single TE-like mode polarization at 1550 nm, a strip waveguide with a height of 220 nm, and width of 440 nm is required. In this case, the waveguide supports one TE-like and one TM-like mode. For wider waveguides, a second TE-like mode is present, and above 660 nm, a second TM-like mode appears. Note that at approximately 680 nm, there is a mode crossing: namely below 680 nm it is the TM-like mode that is the second supported mode of the waveguide, whereas above 680 nm, the TE-like mode becomes the second one and the TM-like mode becomes the third-order mode. The polarization of the mode is also recorded; note that these waveguides do not operate in a pure TE

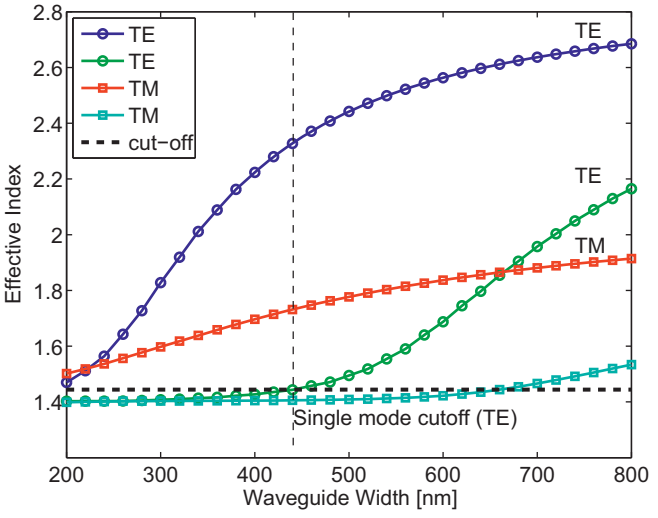

(a) Wavelength of 1550 nm

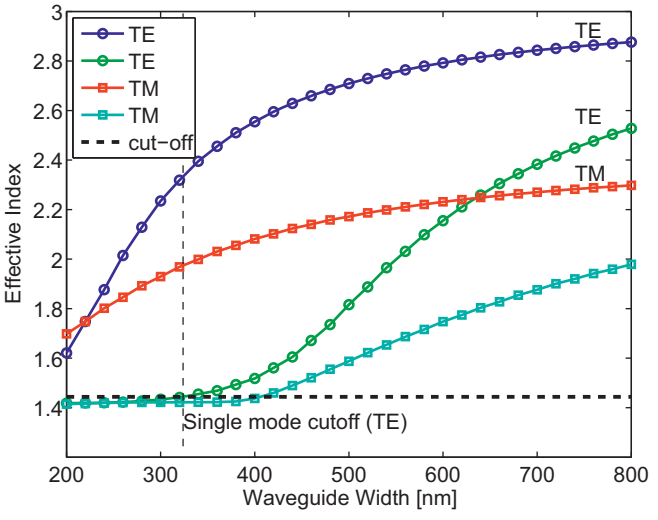

(b) Wavelength of 1310 nm

Figure 3.18 Simulation of the effective index of the waveguide modes versus the width of a strip waveguide, for a silicon thickness of 220 nm.

or TM polarization, hence the polarization is described as a polarization fraction, with 1 representing a pure TE mode. The polarization fraction is plotted in Figure 3.19. It is seen that the fundamental TE-mode polarization fraction is typically between 0.95 and 1 (nearly pure TE mode), whereas the other polarizations are not pure polarizations. This effect can be used design polarization converters, whereby efficient mixing occurs when the TE and TM polarizations have similar effective indices – e.g. at 680 nm, the first TM and second TE modes cross, as shown in Figure 3.18a.

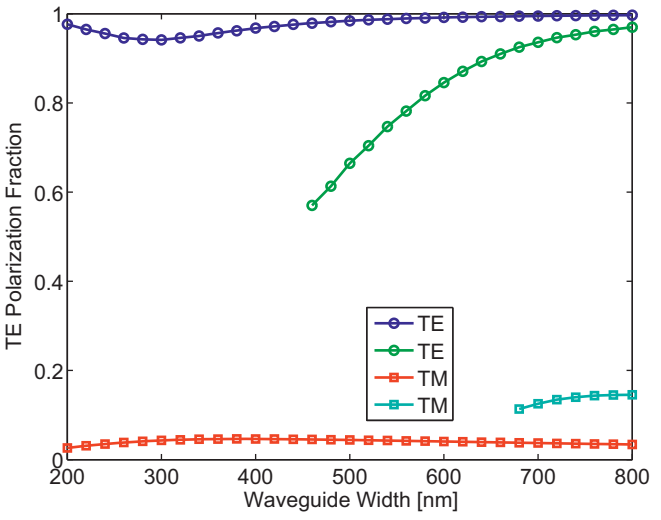

Figure 3.19 Simulation of the mode polarization fraction (relative to a pure TE mode) versus the width of the strip waveguide, for a silicon thickness of 220 nm.

For 1310 nm, the 220 nm thickness is not perfectly single-mode hence there are some weakly guided higher-order slab modes present. Hence, perfectly single-mode operation is not possible. This was already known from the slab waveguide data in Figure 3.10b, where it was found that a thickness of approximately 205 nm is required for single TE-mode operation. Hence, the four modes considered are guided. Despite this, the fundamental TE-like mode is much more confined than the other modes, hence it is still possible to design devices operating at 1310 nm using this waveguide geometry.

We also examine a rib waveguide with a 90 nm slab thickness. The results are shown in Figure 3.20 for a wavelength of 1550 nm. This waveguide does not support any TM modes. This is the type of waveguide used for electro-optic devices such as pn-junction modulators, described in Section 6.2.2.

3.2.9 Wavelength dependence

The wavelength dependence of the waveguide's effective and group index is simulated via Script 3.15. The script performs a sweep of the wavelength. The results for the effective index are shown in Figure 3.21a. The effective index of the waveguide is used to describe the phase velocity of the light, v_p. However, it is the group index that determines the propagation speed of a pulse, namely the group velocity, v_g:

$$v_p(\lambda) = \frac{c}{n_{\text{eff}}}, \quad v_g(\lambda) = \frac{c}{n_{\text{g}}}. \tag{3.4}$$

The group index is an important parameter in photonic integrated circuit design since it is the group index that determines the mode spacing (free-spectral range) in resonators

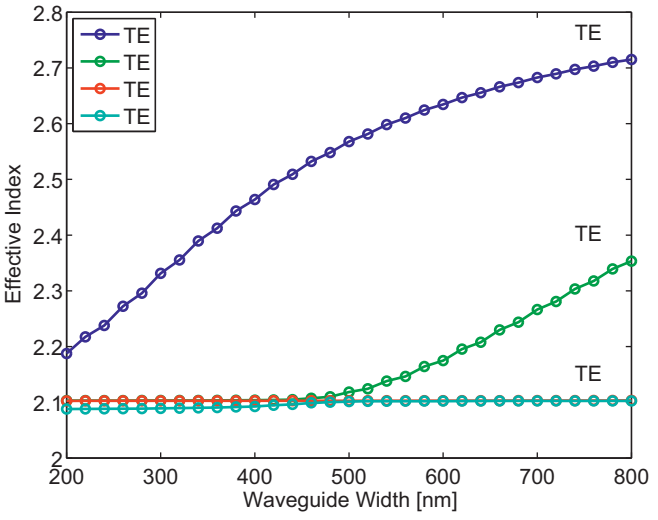

Figure 3.20 Simulation of the effective index of the waveguide modes versus the width of a rib waveguide, for a silicon thickness of 220 nm and slab thickness of 90 nm.

and interferometers. The group index can be related to the effective index:

$$n_g(\lambda) = n_{\text{eff}}(\lambda) - \lambda \frac{dn_{\text{eff}}}{d\lambda}. \tag{3.5}$$

The group index is plotted in Figure 3.21b. The simulated group index is compared with experimental results extracted from a ring resonator. Good agreement is obtained when: (a) a small enough mesh is used to ensure accuracy, in this case 10 nm; (b) both material and waveguide dispersion are taken into account. It is important to include both the material dispersion and waveguide dispersion to correctly predict the group index. Group velocity dispersion, important in understanding the spreading of optical pulses travelling down a waveguide, can also be determined from these simulations by taking the next-order derivative. This is described by the dispersion parameter:

$$\mathrm{D}(\lambda) = \frac{d\frac{n_g}{c}}{d\lambda} = -\frac{\lambda}{c}\frac{d^2 n_{\text{eff}}}{d\lambda^2}. \tag{3.6}$$

Simulations are also performed to illustrate the effect of the waveguide width on the wavelength dependence of the waveguides. The fundamental TE-like mode is considered. The effective index and group index versus wavelength for the 220×550 nm strip waveguide are plotted in Figure 3.22. Similarly, Figure 3.23 is for the rib waveguide with a 90 nm slab.

3.2.10 Compact models for waveguides

For device (e.g. ring resonators) and system design, it is often preferable to describe the performance of the waveguides using compact models consisting of phenomenological

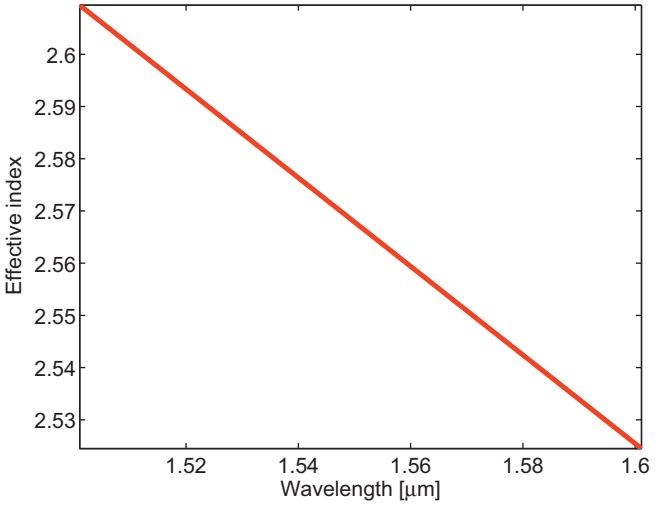

(a) Effective index, rib waveguide

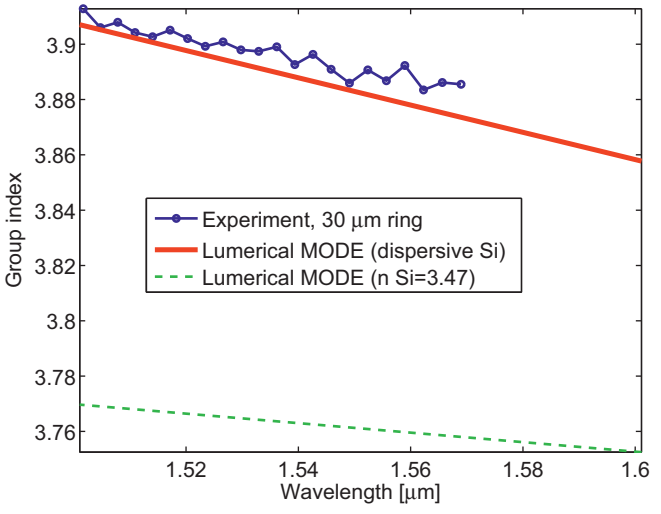

(b) Group index, rib waveguide

Figure 3.21 Simulation of the effective and group index of the rib waveguide versus wavelength, for a silicon thickness of 220 nm with a slab height of 90 nm. Comparison with experimental results (see Section 4.4) for the same geometry are included.

parameters and fit functions. If there is no obvious physical dependency on the parameters, the results can be fitted using Taylor expansion approximations.

For the waveguide in Figure 3.21, the wavelength-dependent effective index can be simply approximated as:

$$n_{\text{eff}}(\lambda) = 2.57 - 0.85(\lambda[\mu\text{m}] - 1.55). \tag{3.7}$$

The waveguide effective index can be calculated for various wavelengths and temperatures, $n_{\text{eff}}(\lambda, T_i)$, and fitted using a second-order Taylor expansion for the wavelength

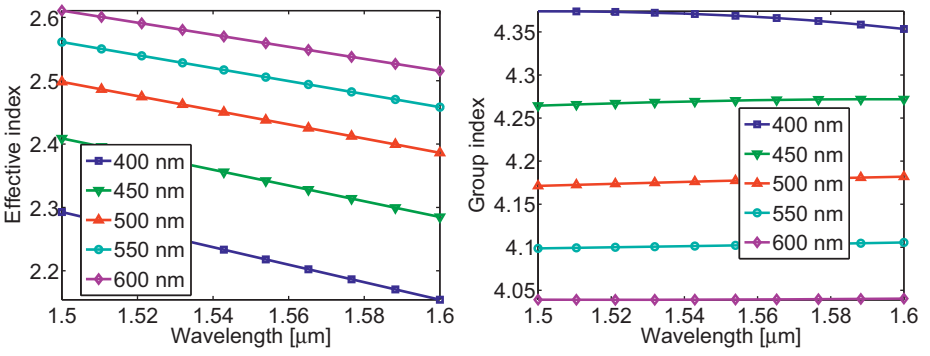

(a) Effective index; strip waveguide (b) Group index; strip waveguide

Figure 3.22 Simulation of the effective and group index of the strip waveguide versus wavelength, for a silicon thickness of 220 nm, for various waveguide widths.

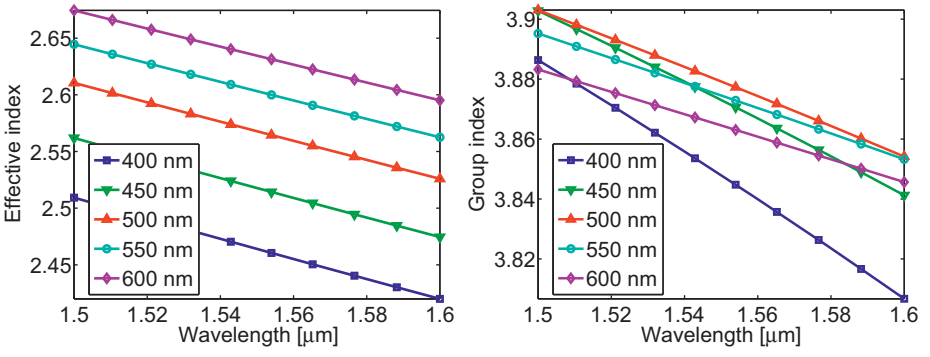

(a) Effective index; rib waveguide (b) Group index; rib waveguide

Figure 3.23 Simulation of the effective and group index of the rib waveguide versus wavelength, for a silicon thickness of 220 nm with a slab height of 90 nm, for various waveguide widths.

λ. Another second-order Taylor expansion for the temperature dependence can then be used. This results in a higher-order polynomial description [19] as follows:

$$n_{\text{eff}}(\lambda,T) = N_0(T) + N_1(T)\left(\tfrac{\lambda-\lambda_0}{\sigma_\lambda}\right) + N_2(T)\left(\tfrac{\lambda-\lambda_0}{\sigma_\lambda}\right)^2$$

$$\begin{cases} N_0(T) &= n_0 + n_1\left(\tfrac{T-T_0}{\sigma_T}\right) + n_2\left(\tfrac{T-T_0}{\sigma_T}\right)^2 \\ N_1(T) &= n_3 + n_4\left(\tfrac{T-T_0}{\sigma_T}\right) + n_5\left(\tfrac{T-T_0}{\sigma_T}\right)^2 \\ N_2(T) &= n_6 + n_7\left(\tfrac{T-T_0}{\sigma_T}\right) + n_8\left(\tfrac{T-T_0}{\sigma_T}\right)^2 \end{cases} . \tag{3.8}$$

The dependence of numerous waveguide parameters can also be included, such as: wavelength, temperature, thickness of the silicon, width of the waveguide, ridge waveguide slab thickness, carrier density, and optical nonlinearity. The designer needs to make a choice regarding the appropriate complexity for the given problem.

A compact model for waveguides that considers the wavelength dependence and the waveguide width is used in the context of synthesizing an optical grating based on a desired spectral response. The design necessarily includes a variation of the width of the waveguide, hence the compact model needs to account for this. This approach is presented in Section 4.5.2.

3.2.11 Waveguide loss

Losses in waveguides originate from several contributions.

- Absorption due to metal in proximity. For example, a 500 × 220 nm strip waveguide with metal above was measured to have an excess loss of 1.8 ± 0.2 dB/cm for metal that is 600 nm above the waveguide.
- Sidewall scattering loss is typically 2–3 dB/cm for 500 × 220 nm waveguides. Atomic force microscope measurements can be done to measure the sidewall roughness. For example, in [20], a 2.8 nm rms roughness was measured. Knowing the roughness, the loss in waveguides can be simulated [21–24].
- Material loss is typically negligible for passive structures. It becomes significant for doped silicon, as described in Section 6.1.1.
- Surface-state absorption can also contribute to the propagation loss if the waveguides are not properly passivated. Indeed, un-passivated waveguides have been used to make detectors [25, 26].
- Sidewall roughness also introduces reflections along the waveguide and phase perturbations that are wavelength dependent [27].

Waveguide losses can be reduced by using wider waveguides, though care has to be taken in single-mode applications since these waveguides are multi-mode. Hence, they require gradual tapers to convert from single-mode to the wide multi-mode waveguide. For example, in Reference [28], the authors report 0.27 dB/cm losses in 2 μm wide, 250 nm high, rib waveguides. Such waveguides are well suited for long-distance traces, e.g. global routing on-chip.

The loss of a waveguide is typically expressed in dB/cm, but can converted to an absorption coefficient, in $[m^{-1}]$, or in terms of the imaginary coefficient, k, in the complex index of refraction, $n + ik$,

$$\alpha[m^{-1}] = \frac{\alpha[\text{dB/m}]}{10\log_{10}(e)} = \frac{\alpha[\text{dB/m}]}{4.34} \tag{3.9a}$$

$$k = \frac{\lambda \cdot \alpha[\text{dB/m}]}{4\pi \cdot 4.34}. \tag{3.9b}$$

3.3 Bent waveguides

A requirement for silicon photonics is to bend waveguides, e.g. for signal routing, and ring/racetrack resonators. Thus, we must understand how much optical loss is introduced by the bend. In this section, we model the bend losses using 3D FDTD.

We determine the relative contributions of radiation loss versus mode mismatch loss using an eigenmode solver. Finally, we compare with experimental data.

There are several mechanisms for loss in bends.

(1) Scattering losses and substrate leakage: for the short distances considered in bends, these losses are small. As we will find, these losses are small for bend radii $<10\,\mu m$.
(2) Radiative loss: in highly confined waveguides, especially for TE modes in strip waveguides, radiation is typically small. It does contribute in rib waveguides for bend radii $<5\,\mu m$ and for TM-polarized modes.
(3) Mode mismatch loss: this is the largest source of loss in bends. It is due to the imperfect mode overlap between the straight and the bent waveguides. This leads to scattering at the abrupt radius transition regions (start and end of fixed-radius bends). There are several methods of decreasing mode-mismatch loss: (a) to laterally offset the straight waveguide relative to the bent waveguide in order to obtain a better mode overlap [29]; (b) to vary the curvature continuously, rather than abruptly; for example a 90° bend with an effective radius of 20 μm, where curvature changes from zero to $1/15\,\mu m^{-1}$ then back to zero [30]. This has the added benefit that the bend does not excite higher order modes in the waveguide. See Figures 10.6, 10.7, and 10.8, for more details.

There have been several reports of losses in bends. For 500 × 220 nm strip waveguides, IBM measured losses per 90° bend to be approximately 0.09 dB for a bending radius of 1 μm and 0.02 dB for a 2 μm bend [29]. Similarly, 500 × 220 nm strip waveguides fabricated at imec, Belgium, demonstrated losses of 0.1 dB per 90° bend for a bending radius of 1 μm and 0.01 dB per 90° bend for a bending radius of 5 μm [31]. It was concluded that the bend loss is decreased to the point where it equals the waveguide propagation loss at a radius of approximately 10 μm [31].

The experimental results presented in this section are based on waveguides fabricated at IME, Singapore, via the OpSIS foundry service. Optical measurements are taken on numerous test structures consisting of two bends (with radius ranging from 0.5 μm to 50 μm, both strip and rib waveguides), where the optical input–output is accessed via fibre grating couplers. The experimental results are shown for both strip (Figures 3.24) and rib (Figures 3.25) waveguides. The experimental data have an uncertainty of approximately 0.2 dB (hence data for larger bends are not reliable). Note: the radius is defined from the centre of the waveguide.

3.3.1 3D FDTD bend simulations

The bend loss can be simulated by 3D FDTD. The scripts in Listings 3.16 and 3.17 draw the input, output, and bent waveguides, define the simulation volume and parameters, add an optical mode source in the waveguide, and add optical power monitors.

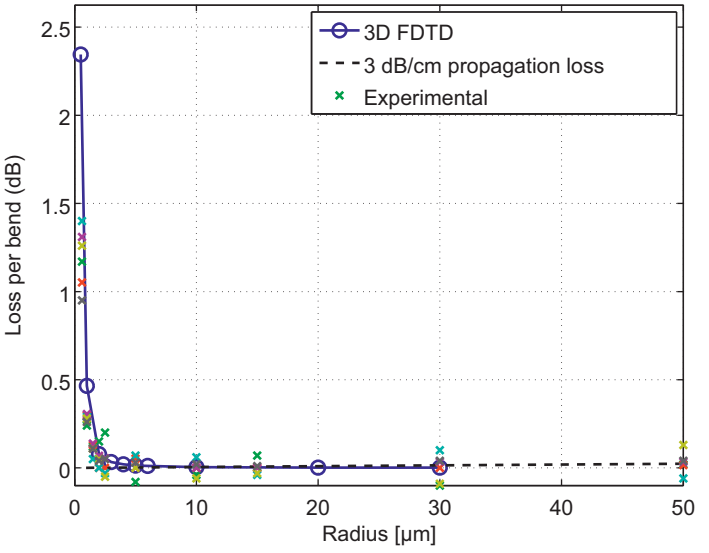

(a) dB scale

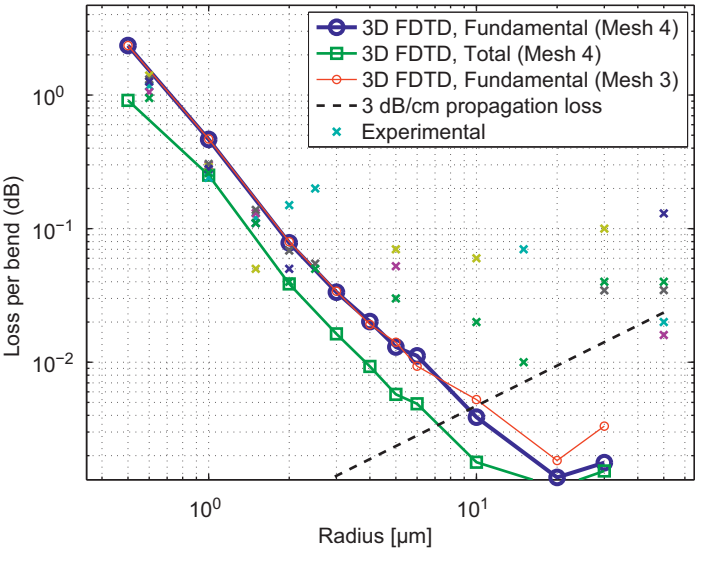

(b) log dB scale

Figure 3.24 Experimental waveguide bend loss versus radius for 500 × 220 nm strip waveguides. Data from OpSIS-IME [32] and 3D FDTD simulation data.

Included is a mode expansion power monitor to determine the power transmitted into the fundamental mode only. The script optionally creates a movie of simulation.

Next, several FDTD simulations are performed, with varied bend radius, in Listing 3.18. A mesh accuracy of 3 and 4 is employed. The optical transmission, defined as

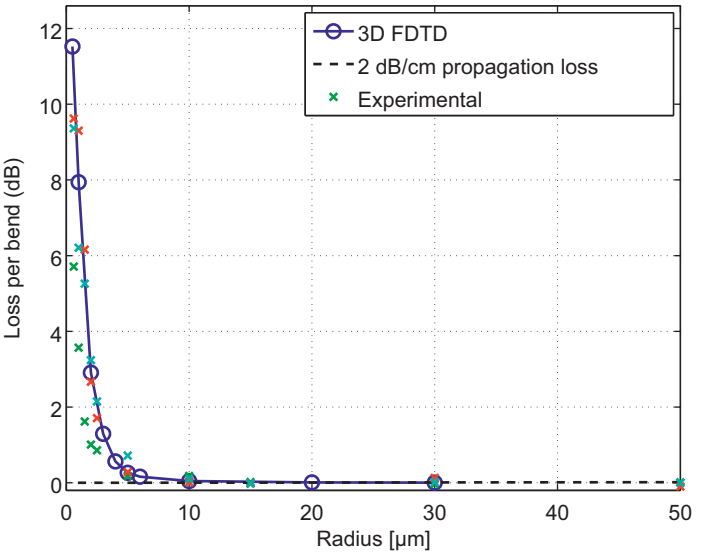

(a) dB scale

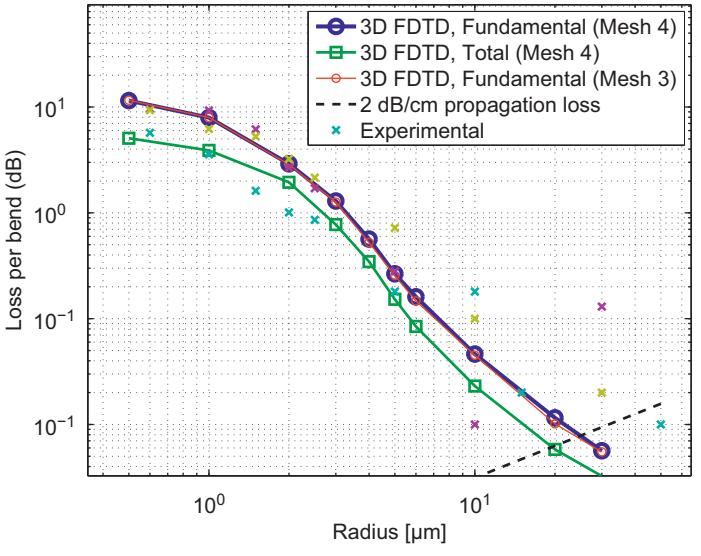

(b) log dB scale

Figure 3.25 Experimental waveguide bend loss versus radius for 500 × 220 nm rib waveguides with a 90 nm slab. Data from OpSIS-IME [32] and 3D FDTD simulation data.

the ratio of the output versus the input, is calculated and plotted versus the bend radius. The transmission can be measured by two methods.

(1) Total transmission: this is a measurement of all the optical power in the output waveguide, hence it includes the power that is not guided in the fundamental

mode. This measurement underestimates the true optical losses of the device. It is included in Figures 3.24 and 3.25 as "3D FDTD, Total".

(2) Fundamental mode transmission: this is a measurement of the optical power in the fundamental mode of the output waveguide. The rationale is that the higher-order modes will scatter away as they propagate down the waveguide, or will be filtered by other mode-selective components (e.g. fibre grating couplers, directional couplers). This measurement is accomplished by performing mode overlap calculations between the FDTD-calculated field and the waveguide mode profile, as described in Reference [33]. It is included in Figures 3.24 and 3.25 as "3D FDTD, Fundamental".

The results for the strip waveguides are plotted together with the experimental results in Figure 3.24. An excellent agreement between the model and the experiments is obtained for the small radius bends (0.5–1 μm), where the losses are large, as shown in Figure 3.24b. For larger radii, the experimental uncertainty is much larger than the predicted losses. On this graph, a line is included for the optical scattering losses, assuming 3 dB/cm. Using the intersection of this propagation loss line, and the 3D FDTD results, the simulations predict that the lowest losses for this conventional 90° bend will be obtained for a 10 μm bend radius.

Similarly, the results for rib waveguides are plotted together with the experimental results in Figure 3.25. Good agreement between the model and the experiments is obtained for radii up to 4 μm, where the losses are large, as shown in Figure 3.25b. For larger radii, the experimental uncertainty is larger than the predicted losses. On this graph, a line is included for the optical scattering losses, assuming 2 dB/cm. The simulations predict that the lowest losses for this conventional 90° bend will be obtained for a 25 μm bend radius.

It should be noted that the inclusion of the dB/cm propagation loss, and the values chosen, are based on the straight waveguide propagation loss. Bent waveguides are known to have higher propagation losses [34]. Hence, the optimal bend radius is likely smaller than stated above.

Next, we are interested in visualizing where the energy is being lost in the bend. This can be done by creating a movie, as in previous script, or by observing the time-integrated E-field intensity, as defined by:

$$|E|^2 = |E_x|^2 + |E_y|^2 + |E_z|^2. \tag{3.10}$$

The script in Listing 3.19 adds a power monitor in the cross-section of the waveguide. The results for the 1 μm bend radius strip waveguide are shown in Figure 3.26, which illustrates where the energy is being lost in the bend.

3.3.2 Eigenmode bend simulations

To understand the loss mechanism, another tool is at our disposal – the waveguide mode eigensolver (Section 2.1) can be used to calculate the field profile of a bent waveguide.

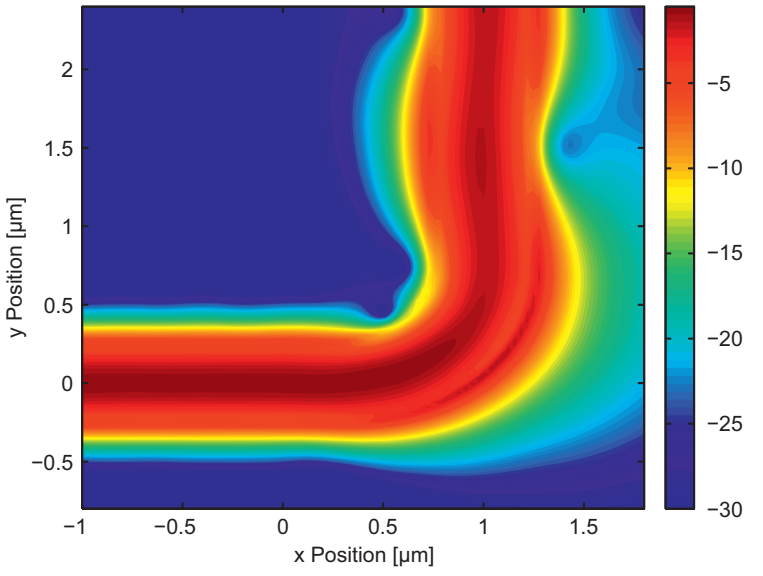

Figure 3.26 Time-integrated field profile of a 90° bend with a radius of 1 μm. Mesh accuracy = 3.

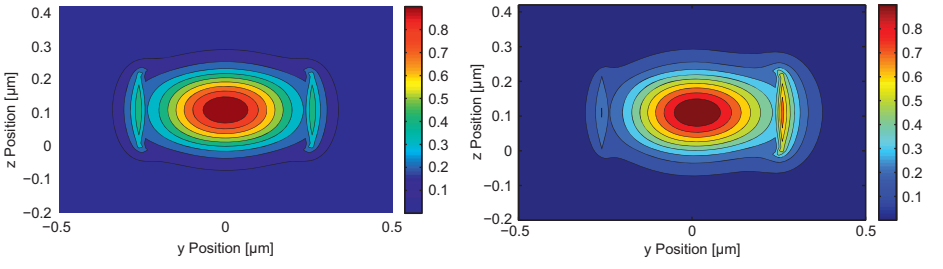

(a) Straight waveguide; linear scale

(b) Bent waveguide; linear scale

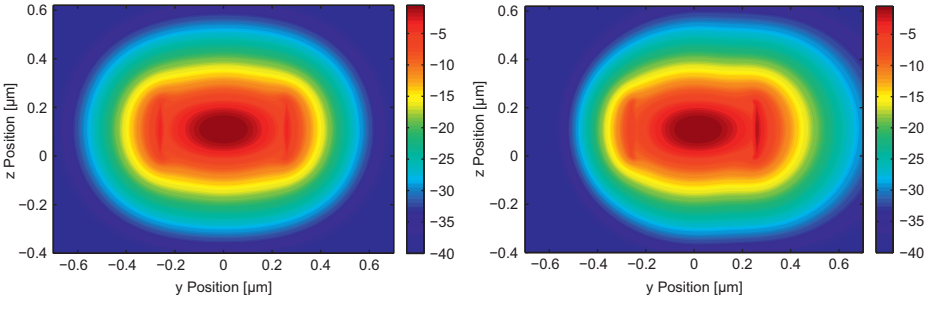

(c) Straight waveguide; log scale

(d) Bent waveguide; log scale

Figure 3.27 E-field mode profile (linear, log scale) of a straight waveguide, 500 × 220 nm strip (left), and the same waveguide bent at a radius of 2 μm (right).

The first portion of Script 3.20 calculates the field profiles for the straight waveguide, as well as for various bent waveguide radii. The field profiles are shown in Figure 3.27. The difference in the field profiles of the straight and bent waveguides is clearly visible and leads to mode-mismatch loss.

The second portion of Script 3.20 calculates mode overlap integrals to determine the power coupled from the straight waveguide to the bent waveguides. Further details on the approach can be found in Reference [35]. The mode calculations for bent waveguides with radii smaller than 3 μm are numerically challenging, hence only results above 3 μm are found.

The results of the mode power coupling calculations are plotted in Figure 3.28a for the strip waveguide and Figure 3.28b for the rib waveguide. For the strip waveguide, negligible radiation loss was found, and the simulations predict that the losses originate from the mode mismatch. However, the predicted losses from the mode calculations are higher than experiments and FDTD simulations. For the rib waveguides, the mode-mismatch losses still dominate over radiation losses; however, radiation losses do contribute significantly for radii below 4 μm. Better agreement between FDTD, experiments, and mode calculations is found in the case of the rib waveguides.

In summary, both the 3D FDTD and eigenmode solver techniques are most suitable for evaluating the loss of bends in waveguides, and the simulations agree well with experimental results.

3.4 Problems

3.1 Find the group and phase velocity of light for the fundamental TE and TM modes in the following waveguides:

- slab waveguide, 220 nm thick, at 1550 nm;
- slot waveguide, in a 500 nm wide strip, with a 150 nm fully etched gap in the middle.

3.2 What is the single-mode condition for the rib waveguide TE mode, for a slab thickness of 90 nm? What is the maximum width for the waveguide before it supports more than one mode? What is the minimum width for the silicon before it does not support a mode?

3.3 Design a single-mode (TE/TM) waveguide for 1310 nm operation, for a silicon thickness of 150 nm, and 220 nm.

3.4 Explain intuitively why the effective index of a strip waveguide typically decreases with wavelength.

3.5 Explain intuitively why the effective index of a strip waveguide typically increases as the waveguide width is increased.

3.6 Explain intuitively why the group index of a strip waveguide typically decreases as the waveguide width is increased (e.g. from 400 nm to 600 nm).

3.7 Design a waveguide with zero group velocity dispersion at 1550 nm.

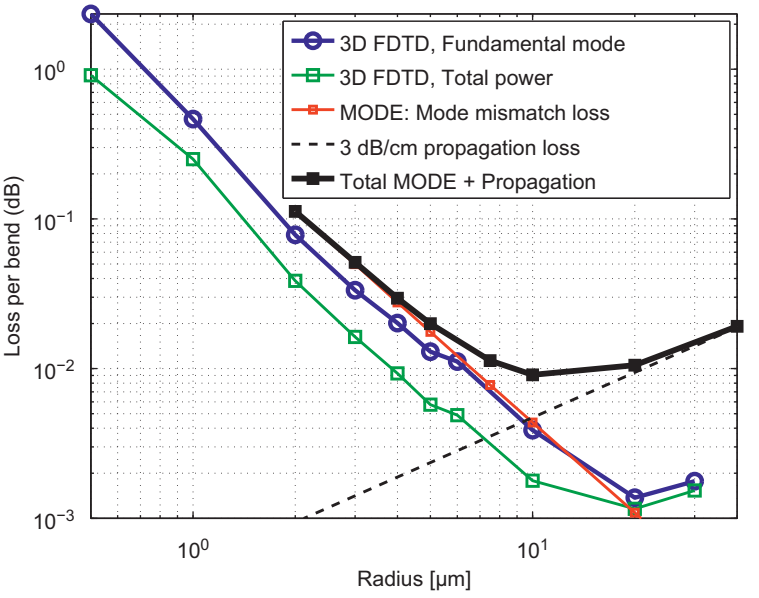

(a) Bend loss for 500 × 220 nm strip waveguides.

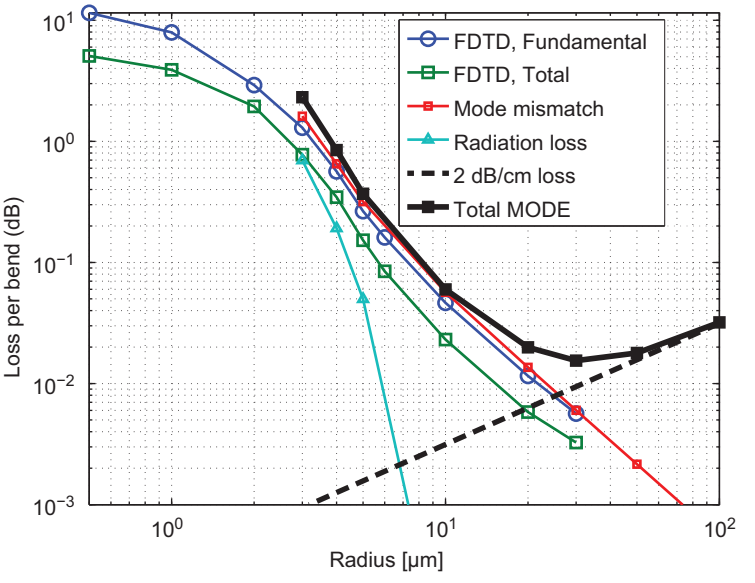

(b) Bend loss for 500 × 220 nm rib waveguides with a 90 nm slab.

Figure 3.28 Numerical waveguide bend loss versus bend radius. Comparison of 3D FDTD results with MODE calculations. MODE simulations can be used to identify the contribution mechanisms: radiation losses are negligible and are dominated by mode-mismatch losses between the straight and bent waveguides. For very large radius bends, the propagation losses (scattering, substrate leakage, etc.) become dominant.

3.5 Code listings

Listing 3.1 Material definitions for Lumerical MODE and FDTD Solutions; materials.lsf

```
# materials.lsf - creates a dispersive material model in Lumerical.
matname = "Si (Silicon) - Dispersive & Lossless";
newmaterial = addmaterial("Lorentz");
setmaterial(newmaterial,"name",matname);
setmaterial(matname,"Permittivity",7.98737492);
setmaterial(matname,"Lorentz Linewidth",1e8);
setmaterial(matname,"Lorentz Resonance",3.93282466e+15);
setmaterial(matname,"Lorentz Permittivity",3.68799143);
setmaterial(matname,"color",[0.85, 0, 0, 1]); # red

matname = "Air (1)";
if (1) { newmaterial = addmaterial("Dielectric"); }
setmaterial(newmaterial,"name",matname);
setmaterial(matname,"Refractive Index",1);
setmaterial(matname,"color",[0.85, 0.85, 0, 1]);

matname = "SiO2 (Glass) - Dispersive & Lossless";
newmaterial = addmaterial("Lorentz");
setmaterial(newmaterial,"name",matname);
setmaterial(matname,"Permittivity",2.119881);
setmaterial(matname,"Lorentz Linewidth",1e10);
setmaterial(matname,"Lorentz Resonance",3.309238e+13);
setmaterial(matname,"Lorentz Permittivity", 49.43721);
setmaterial(matname,"color",[0.5, 0.5, 0.5, 1]); # grey

matname = "SiO2 (Glass) - Const";
newmaterial = addmaterial("Dielectric");
setmaterial(newmaterial,"name",matname);
setmaterial(matname,"Permittivity",1.444^2);
setmaterial(matname,"color",[0.5, 0.5, 0.5, 1]); # grey
```

Listing 3.2 Analytic calculation of 1D waveguide mode parameters and effective index, in MATLAB; see Section 3.2 in *Photonics: Optical Electronics in Modern Communication* by A. Yariv and P. Yeh, 6th edition, Equations 3.2-1 to 3.2-5 [36]; wg_1D_analytic.m

```
% wg_1D_analytic.m - Analytic solution of waveguide
% by Lumerical Solutions, http://www.lumerical.com/mode_online_help/slab_wg.m
% modified by Lukas Chrostowski, 2012
% See Yariv Photonics book, Chapter 3
% finds the TE and TM effective indices of a 3-layer waveguide

% usage:
%  - get effective indices for supported modes:
%  [nTE, nTM] = wg_1D_analytic2 (1.55e-6, 0.22e-6, 1.444, 3.47, 1.444)
%  - TEparam,TMparam: h, q, p parameters of the mode.

function [nTE,nTM,TEparam,TMparam]=wg_1D_analytic (lambda, t, n1, n2, n3)
k0 = 2*pi/lambda;
b0 = linspace( max([n1 n3])*k0, n2*k0, 1000); %k0*n3 < b < k0*n2
b0 = b0(1:end-1);
te0=TE_eq(b0,k0,n1,n2,n3,t);
tm0=TM_eq(b0,k0,n1,n2,n3,t);

%TE
intervals=(te0>=0)-(te0<0);
izeros=find(diff(intervals)<0);
X0=[b0(izeros); b0(izeros+1)]';
[nzeros,scrap]=size(X0);
for i=1:nzeros
    nTE(i)=fzero(@(x) TE_eq(x,k0,n1,n2,n3,t),X0(i,:))/k0;
    [TEparam(i,1),TEparam(i,2),TEparam(i,3),TEparam(i,4)]= TE_eq(nTE(i)*k0,k0,n1,n2,n3,t);
end
nTE=nTE(end:-1:1);
TEparam=TEparam(end:-1:1,:);
```

```
%TM
intervals=(tm0>=0)-(tm0<0);
izeros=find(diff(intervals)<0);
X0=[b0(izeros); b0(izeros+1)]';
[nzeros,scrap]=size(X0);
for i=1:nzeros
    nTM(i)=fzero(@(x) TM_eq(x,k0,n1,n2,n3,t),X0(i,:))/k0;
    [TMparam(i,1),TMparam(i,2),TMparam(i,3),TMparam(i,4)]= TM_eq(nTM(i)*k0,k0,n1,n2,n3,t);
end
if nzeros>0
    nTM=nTM(end:-1:1);
    TMparam=TMparam(end:-1:1,:);
else
    nTM=[];
end

function [te0,h0,q0,p0]=TE_eq(b0,k0,n1,n2,n3,t)
h0 = sqrt( (n2*k0)^2 - b0.^2 );
q0 = sqrt( b0.^2 - (n1*k0)^2 );
p0 = sqrt( b0.^2 - (n3*k0)^2 );
%the objective is to find zeroes of te0 and tm0
te0 = tan( h0*t ) - (p0+q0)./h0./(1-p0.*q0./h0.^2);

function [tm0,h0,q0,p0]=TM_eq(b0,k0,n1,n2,n3,t)
h0 = sqrt( (n2*k0)^2 - b0.^2 );
q0 = sqrt( b0.^2 - (n1*k0)^2 );
p0 = sqrt( b0.^2 - (n3*k0)^2 );
pbar0 = (n2/n3)^2*p0;
qbar0 = (n2/n1)^2*q0;
tm0 = tan( h0*t ) - h0.*(pbar0+qbar0)./(h0.^2-pbar0.*qbar0);
```

Listing 3.3 Analytic calculation of 1D waveguide field profile, in MATLAB; see Section 3.2 in *Photonics: Optical Electronics in Modern Communication* by A. Yariv and P. Yeh, 6th edition, Equations 3.2-2 to 3.2-7 [36]; wg_1D_mode_profile.m

```
% wg_1D_mode_profile.m - Calculate the 1D mode profile of a waveguide
% by Lukas Chrostowski, 2012
% See Yariv Photonics book, Chapter 3.2
% - function returns mode profiles for TE and TM modes (E, H components)
% usage, e.g.:
%  [x, TE_E, TE_H, TM_E, TM_H] = wg_1D_mode_profile (1.55e-6, 0.22e-6, 1.444, 3.47, 1.444,
      100, 4)
%  plot (x, TE_E);

function [x, TE_E, TE_H, TM_E, TM_H]= wg_1D_mode_profile (lambda, t, n1, n2, n3, pts, M)
[nTE,nTM,TEparam,TMparam]= wg_1D_analytic(lambda,t,n1,n2,n3);
x1=linspace( -M*t, -t/2, pts); x2=linspace( -t/2, t/2, pts);
x3=linspace( t/2, M*t, pts); x=[x1 x2 x3];
nx=[n1*ones(pts,1); n2*ones(pts,1); n3*ones(pts,1)]';
mu0=4*pi*1e-7; epsilon0=8.85e-12; eta=sqrt(mu0/epsilon0); c=3e8; % constants
for i=1:length(nTE)
    h=TEparam(i,2);q=TEparam(i,3); p=TEparam(i,4);
    beta = 2*pi*nTE(i)/lambda;
    C=2*h*sqrt ( 2*pi*c/lambda*mu0 / (beta * (t+1/q+1/p)*(h^2+q^2) ) ); % normalize to 1W
    % n1, n2, n3 regions
    TE_E(i,:)=C*[exp(q*(x1+t/2)), (cos(h*(x2+t/2))+q/h*sin(h*(x2+t/2))),
         (cos(h*t)+q/h*sin(h*t)).*exp(-p*(x3-t/2))];
end
TE_H=TE_E'.*(nx'*ones(1,length(nTE)))/eta;

for i=1:length(nTM)
    h=TMparam(i,2); q=TMparam(i,3);
    p=TMparam(i,4); qb=n2^2/n1^2*q;pb=n2^2/n3^2*p;
    beta = 2*pi*nTM(i)/lambda;
    temp=(qb^2+h^2)/qb^2 * (t/n2^2 + (q^2+h^2)/(qb^2+h^2)/n1^2/q + (
         p^2+h^2)/(p^2+h^2)/n3^2/p) ;
```

```
    C=2*sqrt ( 2*pi*c/lambda*epsilon0 / (beta * temp )); % normalize to 1W
    TM_H(i,:)=C*[h/qb*exp(q*(x1+t/2)), (h/qb*cos(h*(x2+t/2))+sin(h*(x2+t/2))),
         (h/qb*cos(h*t)+sin(h*t)).*exp(-p*(x3-t/2))];
end
TM_E=TM_H'./(nx'*ones(1,length(nTM)))*eta;
```

Listing 3.4 Draw the 2D waveguide structure, in Lumerical MODE Solutions; wg_2D_draw.lsf

```
# wg_2D_draw.lsf - draw the waveguide geometry in Lumerical MODE
newmode; newmode; redrawoff;

# define wafer and waveguide structure
thick_Clad = 2.0e-6;
thick_Si  = 0.22e-6;
thick_BOX = 2.0e-6;
thick_Slab = 0;               # for strip waveguides
# thick_Slab = 0.13e-6;       # for rib waveguides
width_ridge = 0.5e-6;         # width of the waveguide

# define materials
material_Clad = "SiO2 (Glass) - Const";
material_BOX = "SiO2 (Glass) - Const";
material_Si  = "Si (Silicon) - Dispersive & Lossless";
materials;    # run script to add materials

# define simulation region
width_margin = 2.0e-6; # space to include on the side of the waveguide
height_margin = 1.0e-6; # space to include above and below the waveguide

# calculate simulation volume
# propagation in the x-axis direction; z-axis is wafer-normal
Xmin = -2e-6; Xmax = 2e-6; # length of the waveguide
Zmin = -height_margin; Zmax = thick_Si + height_margin;
Y_span = 2*width_margin + width_ridge; Ymin = -Y_span/2; Ymax = -Ymin;

# draw cladding
addrect; set("name","Clad"); set("material", material_Clad);
set("y", 0);            set("y span", Y_span+1e-6);
set("z min", 0);        set("z max", thick_Clad);
set("x min", Xmin);     set("x max", Xmax);
set("override mesh order from material database",1);
set("mesh order",3); # similar to "send to back", put the cladding as a background.
set("alpha", 0.05);

# draw buried oxide
addrect; set("name", "BOX"); set("material", material_BOX);
set("x min", Xmin);     set("x max", Xmax);
set("z min", -thick_BOX); set("z max", 0);
set("y", 0);            set("y span", Y_span+1e-6);
set("alpha", 0.05);

# draw silicon wafer
addrect; set("name", "Wafer"); set("material", material_Si);
set("x min", Xmin);     set("x max", Xmax);
set("z max", -thick_BOX); set("z min", -thick_BOX-2e-6);
set("y", 0);            set("y span", Y_span+1e-6);
set("alpha", 0.1);

# draw waveguide
addrect; set("name", "waveguide"); set("material",material_Si);
set("y", 0);      set("y span", width_ridge);
set("z min", 0);  set("z max", thick_Si);
set("x min", Xmin); set("x max", Xmax);

# draw slab for rib waveguides
addrect; set("name", "slab"); set("material",material_Si);
if (thick_Slab==0) {
 set("y min", 0);   set("y max", 0);
```

```
} else {
 set("y", 0);       set("y span", Y_span+1e-6);
}
set("z min", 0);    set("z max", thick_Slab);
set("x min", Xmin); set("x max", Xmax);
set("alpha", 0.2);
```

Listing 3.5 One-dimensional slab waveguide simulation parameters, in Lumerical MODE Solutions; wg_1D_slab.lsf

```
# wg_1D_slab.lsf - setup the Lumerical MODE 1D simulation

wg_2D_draw;             # draw the waveguide

wavelength=1.55e-6;
meshsize = 10e-9; # mesh size

# add 1D mode solver (waveguide cross-section)
addfde; set("solver type","1D Z:X prop");
set("x", 0); set("y", 0);
set("z max", Zmax); set("z min", Zmin);
set("wavelength", wavelength);
set("define z mesh by","maximum mesh step");
set("dz", meshsize);
modes=2; # modes to output
set("number of trial modes",modes);
```

Listing 3.6 One-dimensional slab waveguide simulation of the mode profile, in Lumerical MODE Solutions; wg_1D_slab_mode.lsf

```
# wg_1D_slab_mode.lsf - calculate mode profiles in Lumerical MODE

wg_1D_slab;    # Draw waveguides and setup the simulation

n=findmodes;   # calculate the modes
for (m=1:modes) {
  ? neff=getdata ("FDE::data::mode"+num2str(m),"neff"); # display effective index
  z=getdata("FDE::data::mode1","z");
  E3=pinch(getelectric("FDE::data::mode"+num2str(m)));
  plot(z,E3); # plot the mode profile
}
```

Listing 3.7 One-dimensional slab waveguide simulation convergence test (for the simulation span), in Lumerical MODE Solutions; wg_1D_slab_convergence_z.lsf

```
# wg_1D_slab_convergence_z.lsf - perform convergence test, Lumerical MODE

wg_1D_slab;    # Draw waveguides and setup the simulation

zspan_list=[.4:0.2:2]*1e-6;  # sweep for the simulation region
neff=matrix(length(zspan_list),2); # initialize empty matrix
for (x=1:length(zspan_list)) {
  switchtolayout;
  select("MODE");
  set("z span", zspan_list(x));
  n=findmodes;
  neff(x,1)=getdata ("MODE::data::mode1","neff");
  neff(x,2)=getdata ("MODE::data::mode2","neff");
}
plot(zspan_list,real(neff)); legend('Mode 1','Mode 2');
matlabsave ('out/wg_slab_convergence_z');
```

Listing 3.8 One-dimensional slab waveguide simulation convergence test (for the simulation mesh), in Lumerical MODE Solutions; wg_1D_slab_convergence_mesh.lsf

```
# wg_1D_slab_convergence_mesh.lsf - perform convergence test, Lumerical MODE

wg_1D_slab;     # Draw waveguides and setup the simulation

mesh_list=[0.01; 0.1; 1:1:50]*1e-9;      # vary the mesh size
refine_list=[1,3];              # 1=Staircase, 3=Conformal mesh
neff=matrix(length(mesh_list),length(refine_list));
for (y=1:length(refine_list)) {
  switchtolayout; select ("MODE"); set ("z span",2e-6);
  set ("mesh refinement", refine_list(y));
  for (x=1:length(mesh_list)) {
    switchtolayout; select("MODE"); set("dz", mesh_list(x));
    n=findmodes;
    neff(x,y)=getdata ("MODE::data::mode1","neff");
  }
}
plot(mesh_list,real(neff)); legend("Staircase mesh","Conformal mesh");
matlabsave ('out/wg_slab_convergence_mesh');
```

Listing 3.9 One-dimensional slab waveguide simulation, for slab thickness parameter sweep, in Lumerical MODE Solutions; wg_1D_slab_neff_sweep.lsf

```
# wg_1D_slab_neff_sweep.lsf - perform sweep mode calculations on the slab

wg_1D_slab;     # Draw waveguides and setup the simulation

thick_Si_list = [0:.01:.4]*1e-6; # sweep waveguide thickness
mode_list=[1:4];

neff_slab = matrix (length(thick_Si_list), length(mode_list) );
TE_pol = matrix (length(thick_Si_list), length(mode_list) );

select("MODE");
set("number of trial modes",max(mode_list)+2);

for(kk=1:length(thick_Si_list))
{
  switchtolayout;
  setnamed('waveguide','z max', thick_Si_list(kk));
  n=findmodes;
  for (m=1:length(mode_list))
  {
    neff_slab (kk,m) =abs( getdata ("MODE::data::mode"+num2str(m),"neff") );
    TE_pol(kk,m) = getdata("MODE::data::mode"+num2str(m),"TE polarization fraction");
    if ( TE_pol(kk,m) > 0.5 )
      {    pol = "TE"; } else  {  pol = "TM"; }
   }
}
plot ( thick_Si_list, neff_slab);
# matlabsave ("wg_mode_neff_sweep_slab"); # save the data for plotting in Matlab.
```

Listing 3.10 Waveguide Effective Index Method; wg_EIM.lsf

```
# wg_EIM.lsf - setup the Lumerical MODE 1D simulation for Effective index method

wg_2D_draw;             # draw the waveguide

material_Si  = "<Object defined dielectric>";
select("waveguide");
set("material",material_Si);
set("index", 2.845); # effective index taken from the TE slab mode
```

```
wavelength=1.55e-6;
meshsize = 10e-9; # mesh size

# add 1D mode solver (horizontal waveguide cross-section)
addfde; set("solver type","1D Y:X prop");
set("x", 0); set("z", 0.1e-6);
set("y max", 1e-6); set("y min", -1e-6);
set("wavelength", wavelength);
set("define y mesh by","maximum mesh step");
set("dy", meshsize);
modes=2; # modes to output
set("number of trial modes",modes);

n=findmodes;   # calculate the modes
for (m=1:modes) {
  ? neff=getdata ("FDE::data::mode"+num2str(m),"neff"); # display effective index
  y=getdata("FDE::data::mode1","y");
  E3=pinch(getelectric("FDE::data::mode"+num2str(m)));
  plot(y,E3); # plot the mode profile
  matlabsave("wg_EIM"+num2str(m));
}
```

Listing 3.11 Analytic calculation of 2D waveguide field profile using the Effective Index Method from Listing 3.2, in MATLAB; wg_EIM_profile.m

```
% wg_EIM_profile.m - Effective Index Method - mode profile
% Lukas Chrostowski, 2012
% usage, e.g.:
%  wg_EIM_profile (1.55e-6, 0.22e-6, 0.5e-6, 90e-9, 3.47, 1, 1.44, 100, 2)

function wg_EIM_profile (lambda, t, w, t_slab, n_core, n_clad, n_oxide, pts, M)

% find TE (TM) modes of slab waveguide (waveguide core and slab portions):
[nTE,nTM]=wg_1D_analytic (lambda, t, n_oxide, n_core, n_clad);
if t_slab>0
    [nTE_slab,nTM_slab]=wg_1D_analytic (lambda, t_slab, n_oxide, n_core, n_clad);
else
    nTE_slab=n_clad; nTM_slab=n_clad;
end
[xslab,TE_Eslab,TE_Hslab,TM_Eslab,TM_Hslab]=wg_1D_mode_profile (lambda, t, n_oxide,
     n_core, n_clad, pts, M);

figure(1); clf; subplot (2,2,2); Fontsize=9;
plot(TE_Eslab/max(max(TE_Eslab)),xslab*1e9,'LineWidth',2);hold all;
ylabel('Height [nm]','FontSize',Fontsize);
xlabel('E-field (TE)','FontSize',Fontsize);
set(gca,'FontSize',Fontsize,'XTick',[]);
axis tight; a=axis; axis ([a(1)*1.1, a(2)*1.1, a(3), a(4)]);
Ax1 = gca; Ax2 = axes('Position',get(Ax1,'Position'));
get(Ax1,'Position');
nx=[n_oxide*ones(pts,1); n_core*ones(pts,1); n_clad*ones(pts,1)]';
plot (nx, xslab*1e9, 'LineWidth',0.5,'LineStyle','--','parent',Ax2);
a2=axis; axis ([a2(1), a2(2), a(3), a(4)]);
set(Ax2,'Color','none','XAxisLocation','top', 'YTick',[],'TickDir','in');
set(gca,'YAxisLocation','right'); box off;
xlabel('Material Index','FontSize',Fontsize);
set(gca,'FontSize',Fontsize);

% TE-like modes of the etched waveguide (for fundamental slab mode)
%   solve for the "TM" modes:
[nTE,nTM]=wg_1D_analytic (lambda, w, nTE_slab(1), nTE(1), nTE_slab(1));
neff_TEwg=nTM;
[xwg,TE_E_TEwg,TE_H_TEwg,TM_E_TEwg,TM_H_TEwg]=wg_1D_mode_profile (lambda, w, nTE_slab(1),
     nTE(1), nTE_slab(1), pts, M);
```

```
subplot (2,2,3);
plot (xwg*1e9, TM_E_TEwg/max(max(TM_E_TEwg)), 'LineWidth',2,'LineStyle','-');
xlabel('Position [nm]','FontSize',Fontsize);
ylabel('E-field (TM, TE-like mode)','FontSize',Fontsize);
set(gca,'FontSize',Fontsize,'YTick',[]);
axis tight; a=axis; axis ([a(1), a(2), a(3)*1.1, a(4)*1.1]);
Ax1 = gca; Ax2 = axes('Position',get(Ax1,'Position'));
nx=[nTE_slab(1)*ones(pts,1); nTE(1)*ones(pts,1); nTE_slab(1)*ones(pts,1)]';
plot (xwg*1e9, nx, 'LineWidth',0.5,'LineStyle','--','parent',Ax2);
set(Ax2,'Color','none','YAxisLocation','right'); box off;
a2=axis; axis ([a(1), a(2), a2(3), a2(4)]);
ylabel('Slab Effective Index','FontSize',Fontsize);
set(gca,'FontSize',Fontsize);

% Plot the product of the two fields
subplot (2,2,1); Exy=TM_E_TEwg(:,1)*(TE_Eslab(1,:));
contourf(xwg*1e9,xslab*1e9,abs(Exy)/max(max(Exy))')
xlabel ('X (nm)','FontSize',Fontsize);
ylabel ('Y (nm)','FontSize',Fontsize);
set (gca, 'FontSize',Fontsize);
A=axis; axis([A(1)+0.4, A(2)-0.4, A(3)+.2, A(4)-0.2]);
title('Effective Index Method');
% Draw the waveguide:
rectangle ('Position',[-w/2,-t/2,w,t]*1e9, 'LineWidth',1, 'EdgeColor','white')
if t_slab>0
    rectangle ('Position',[-M*w,-t/2,(M-0.5)*w, t_slab]*1e9, 'LineWidth',1,
        'EdgeColor','white')
    rectangle ('Position',[w/2,-t/2,(M-0.5),t_slab]*1e9, 'LineWidth',1,
        'EdgeColor','white')
end

function draw_WG_vertical(M)
pP=get(gca,'Position');pPw=pP(3);
pPc=pP(3)/2+pP(1); pP2=pPw/4/M;
annotation ('line',[pPc-pP2,pPc-pP2], [pP(2),pP(4)+pP(2)],'LineStyle','--');
annotation ('line',[pPc+pP2,pPc+pP2], [pP(2),pP(4)+pP(2)],'LineStyle','--');
axis tight; a=axis; axis ([a(1), a(2), a(3)*1.1, a(4)*1.1]);

function draw_WG_horiz(M)
pP=get(gca,'Position');pPw=pP(4);
pPc=pP(4)/2+pP(2); pP2=pPw/4/M;
annotation ('line',[pP(1),pP(3)+pP(1)], [pPc-pP2,pPc-pP2],'LineStyle','--');
annotation ('line',[pP(1),pP(3)+pP(1)], [pPc+pP2,pPc+pP2],'LineStyle','--');
axis tight; a=axis; axis ([a(1)*1.1, a(2)*1.1, a(3), a(4)]);
```

Listing 3.12 Waveguide 2D eigenmode calculation setup; wg_2D.lsf

```
# wg_2D.lsf - set up the mode profile simulation solver

wg_2D_draw;  # run script to draw the waveguide

# define simulation parameters
wavelength   = 1.55e-6;
meshsize     = 20e-9;      # maximum mesh size
modes        = 4;          # modes to output

# add 2D mode solver (waveguide cross-section)
addfde; set("solver type", "2D X normal");
set("x", 0);
set("y", 0);       set("y span", Y_span);
set("z max", Zmax); set("z min", Zmin);
set("wavelength", wavelength); set("solver type","2D X normal");
set("define y mesh by","maximum mesh step"); set("dy", meshsize);
set("define z mesh by","maximum mesh step"); set("dz", meshsize);
set("number of trial modes",modes);
```

Listing 3.13 Waveguide 2D eigenmode profile calculation; wg_2D_mode_profile.lsf

```
# wg_2D_mode_profile.lsf - calculate the mode profiles of the waveguide

wg_2D;  # run the script to draw the waveguide and set up the simulation

# output filename
clad = substring(material_Clad, 1, (findstring(material_Clad,' '))-1);
?FILE = "out/wl" + num2str(wavelength*1e9) +"nm_" + clad + "-clad" +
       "_"+ num2str(thick_Si*1e9) + "nm-wg_" + num2str(thick_Slab*1e9)+"nm-ridge";

# find the material dispersion (using 2 frequency points), for energy density calculation
switchtolayout; set("wavelength", wavelength*(1 + .001) );
run; mesh;
f1 = getdata("FDE::data::material","f");
eps1 = pinch(getdata("FDE::data::material","index_x"))^2;
switchtolayout; set("wavelength", wavelength*(1 - .001) );
run; mesh;
f3 = getdata("FDE::data::material","f");
eps3 = pinch(getdata("FDE::data::material","index_x"))^2;
re_dwepsdw = real((f3*eps3-f1*eps1)/(f3-f1));

switchtolayout; set("wavelength", wavelength);
n=findmodes;
neff = matrix ( modes ); TE_pol = matrix (modes );
for (m=1:modes) {       # extract mode data
  neff(m) = abs( getdata ("FDE::data::mode"+num2str(m),"neff") );
  TE_pol(m) = getdata("FDE::data::mode"+num2str(m),"TE polarization fraction");
  if ( TE_pol(m) > 0.5 ) # identify the TE-like or TM-like modes
    {   pol = "TE"; }   else  {   pol = "TM"; }
  z  = getdata("FDE::data::mode"+num2str(m),"z");
       y=getdata("FDE::data::mode"+num2str(m),"y");
  E1 = pinch(getelectric("FDE::data::mode"+num2str(m)));
  H1 = pinch(getmagnetic("FDE::data::mode"+num2str(m)));
  W1 = 0.5*(re_dwepsdw*eps0*E1+mu0*H1);
  image(y,z,E1);  # plot E-field intensity of mode
  setplot("title","mode" + num2str(m) + "("+pol+"): "+"neff:" + num2str(neff(m)));
  image(y,z,W1); # plot energy density of mode
  setplot("title","mode" + num2str(m) + "("+pol+"): "+"neff:" + num2str(neff(m)));
# matlabsave ( FILE + "_"+ num2str(m) );
}
```

Listing 3.14 Effective index versus waveguide width (2D simulation); wg_2D_neff_sweep_width.lsf

```
# wg_2D_neff_sweep_width.lsf - perform mode calculations on the waveguide

wg_2D;    # run the script to draw the waveguide and set up the simulation

modes=4;         # modes to output
set("number of trial modes",modes+2);

# define parameters to sweep
width_ridge_list=[.2:.02:.8]*1e-6; # sweep waveguide width

neff = matrix (length(width_ridge_list), modes );
TE_pol = matrix (length(width_ridge_list), modes );

for(ii=1:length(width_ridge_list)) {
  switchtolayout;
  setnamed("waveguide","y span", width_ridge_list(ii));
  setnamed("slab","z max", thick_Slab);
  n=findmodes;
  for (m=1:modes) { # extract mode data
    neff (ii,m) = abs( getdata ("FDE::data::mode"+num2str(m),"neff") );
    TE_pol(ii,m) = getdata("FDE::data::mode"+num2str(m),"TE polarization fraction");
  }
}
plot (width_ridge_list, neff (1:length(width_ridge_list), 1)); # plots the 1st mode.
plot (width_ridge_list, neff);
```

Listing 3.15 Effective and group index versus wavelength; wg_2D_neff_sweep_wavelength.lsf

```
# wg_2D_neff_sweep_wavelength.lsf - Calculate the wavelength dependence of waveguide's
     neff and ng

wg_2D; # draw waveguide

run; mesh;
setanalysis('wavelength',1.6e-6);
findmodes; selectmode(1); # find the fundamental mode

setanalysis("track selected mode",1);
setanalysis("number of test modes",5);
setanalysis("detailed dispersion calculation",0); # This feature is useful for
     higher-order dispersion.
setanalysis('stop wavelength',1.5e-6);
frequencysweep;  # perform sweep of wavelength and plot
f=getdata("frequencysweep","f");
neff=getdata("frequencysweep","neff");
f_vg=getdata("frequencysweep","f_vg");
ng=c/getdata("frequencysweep","vg");
plot(c/f*1e6,neff,"Wavelength (um)", "Effective Index");
plot(c/f_vg*1e6,ng,"Wavelength (um)", "Group Index");
matlabsave ('wg_2D_neff_sweep_wavelength.mat',f, neff, f_vg, ng);
```

Listing 3.16 Draw the bent waveguides; bend_draw.lsf

```
# bend_draw.lsf - Define simulation parameters, draw the bend
# input: variable "bend_radius" pre-defined

# define wafer structure
thick_Clad = 3e-6;
thick_Si = 0.22e-6;
thick_BOX = 2e-6;
thick_Slab = 0;         # for strip waveguides
#thick_Slab = 0.09e-6;  # for rib waveguides
width_ridge = 0.5e-6;   # width of the waveguide

# define materials
material_Clad = "SiO2 (Glass) - Const";
material_BOX = "SiO2 (Glass) - Const";
material_Si  = "Si (Silicon) - Dispersive & Lossless";
materials;    # run script to add materials

Extra=0.5e-6;
thick_margin = 500e-9;
width_margin=2e-6;
length_input=1e-6;

Xmin = 0-width_ridge/2-width_margin;
Xmax = bend_radius+length_input;
Zmin =-thick_margin; Zmax=thick_Si+thick_margin;
Ymin = 0;
Ymax = bend_radius+width_ridge/2+width_margin+length_input/2;

addrect; set('name','Clad'); set("material", material_Clad);
set('y min', Ymin-Extra); set('y max', Ymax+Extra);
set('z min', 0);         set('z max', Zmax);
set('x min', Xmin-Extra); set('x max', Xmax+Extra);
set('alpha', 0.2);

addrect; set("name", "BOX"); set("material", material_BOX);
set('x min', Xmin-Extra); set('x max', Xmax+Extra);
set('z min', -thick_BOX); set('z max', 0);
set('y min', Ymin-Extra); set('y max', Ymax+Extra);
set('alpha', 0.3);

addrect; set("name", "slab"); set("material",material_Si);
set('y min', Ymin-Extra); set('y max', Ymax+Extra);
```

```
set('z min', 0);         set('z max', thick_Slab);
set('x min', Xmin-Extra); set('x max', Xmax+Extra);
set('alpha', 0.4);

addrect; set('name', 'input_wg'); set("material",material_Si);
set('x min', -width_ridge/2); set('x max', width_ridge/2);
set('z min', 0);            set('z max', thick_Si);
set('y min', Ymin-2e-6);    set('y max', Ymin+length_input);

addrect; set('name', 'output_wg'); set("material",material_Si);
set('y', length_input+bend_radius); set('y span', width_ridge);
set('z min', 0);         set('z max', thick_Si);
set('x min', bend_radius); set('x max', bend_radius+length_input+2e-6);

addring; set('name', 'bend'); set("material",material_Si);
set('x', bend_radius);
set('y', length_input);
set('z min', 0); set('z max', thick_Si);
set('theta start', 90); set('theta stop', 180);
set('outer radius', bend_radius+0.5*width_ridge);
set('inner radius', bend_radius-0.5*width_ridge);
```

Listing 3.17 Set up the 3D FDTD simulation for bent waveguides; bend_FDTD_setup.lsf

```
# bend_FDTD_setup.lsf - setup FDTD simulation for bend calculations

wavelength=1.55e-6;
Mode_Selection = 'fundamental TE mode';
Mesh_level=1; # Mesh of 3 is suitable for high accuracy

addfdtd;
set('x min', Xmin); set('x max', Xmax);
set('y min', Ymin); set('y max', Ymax);
set('z min', Zmin); set('z max', Zmax);
set('mesh accuracy', Mesh_level);

addmode;
set('injection axis', 'y-axis');
set('direction', 'forward');
set('y', Ymin+100e-9);
set('x', 0); set('x span', width_ridge+width_margin);
set('z min', Zmin); set('z max', Zmax);
set('set wavelength','true');
set('wavelength start', wavelength);
set('wavelength stop',wavelength);
set('mode selection', Mode_Selection);
updatesourcemode;

addpower;  # Power monitor, output
set('name', 'transmission');
set('monitor type', '2D X-normal');
set('y', length_input+bend_radius);
set('y span', width_ridge +width_margin);
set('z min', Zmin); set('z max', Zmax);
set('x', Xmax-0.5e-6);

addmodeexpansion;
set('name', 'expansion');
set('monitor type', '2D X-normal');
set('y', length_input+bend_radius);
set('y span', width_ridge +width_margin);
set('z min', Zmin); set('z max', Zmax);
set('x', Xmax-0.3e-6);
set('frequency points',10);
set('mode selection', Mode_Selection);
setexpansion('T','transmission');

addpower;  # Power monitor, input
set('name', 'input');
```

```
set('monitor type', '2D Y-normal');
set('y', Ymin+500e-9); set('x', 0);
set('x span', width_ridge+width_margin);
set('z min', Zmin); set('z max', Zmax);

if (0) {
  addmovie;
  set('name', 'movie');
  set('lockAspectRatio', 1);
  set('monitor type', '2D Z-normal');
  set('x min', Xmin); set('x max', Xmax);
  set('y min', Ymin); set('y max', Ymax);
  set('z', 0.5*thick_Si);
}
```

Listing 3.18 Run 3D FDTD simulations for bent waveguides; bend_FDTD_radius_sweep.lsf

```
# bend_FDTD_radius_sweep.lsf - 3D-FDTD script to calculate the loss in a 90 degree bend
      versus bend-radius, including mode expansion

bend_radius_sweep=[0.5,1,2,3,4,5,6,10,20,30]*1e-6; # bend radii to sweep

L=length(bend_radius_sweep); T=matrix(2,L);
for(ii=1:L)
{
  newproject; switchtolayout; redrawoff;
  selectall; delete;
  bend_radius = bend_radius_sweep(ii);
  bend_draw;       # draw the waveguides
  bend_FDTD_setup; # setup the FDTD simulations
  save('bend_radius_'+ num2str(ii));
  run;
       T_fund=getresult('expansion', 'expansion for T');
       T_forward=T_fund.getattribute('T forward');
  T(1,ii)=T_forward;
       T(2,ii)=transmission('transmission'); # total output power in WG
       T(3,ii)=transmission('input'); # output power in fundamental mode
}
plot(bend_radius_sweep, -10*log10(T(1,1:ii)/T(3,1:ii)), -10*log10(T(2,1:ii)/T(3,1:ii)));
legend ('Transmission, in fundamental mode', 'Transmission, total');
matlabsave ('bend.mat', bend_radius_sweep, T);
```

Listing 3.19 3D FDTD simulations for bent waveguides to visualize the E-field intensity; bend_FDTD_top_field.lsf

```
# bend_top_field.lsf - simulate a bend, observe the top-view field profile

bend_radius = 1e-6;  # 1 micron bend radius
bend_draw;           # Call script to draw the bent waveguide
bend_FDTD_setup;     # setup the FDTD simulations

addpower;  # Power monitor, top-view
set('name', 'top');
set('monitor type', '2D Z-normal');
set('x min', Xmin); set('x max', Xmax);
set('y min', Ymin); set('y max', Ymax);
set('z', thick_Si/2); # cross-section through the middle of the waveguide

save('./out/bend_FDTD_top_field');
run;

X=getdata('top','x'); Y=getdata('top','y');
I2=abs(getdata('top','Ex'))^2 + abs(getdata('top','Ey'))^2 + abs(getdata('top','Ez'))^2;
image(X,Y,I2);          # E-field intensity image plot
image(X,Y,10*log10(I2)); # E-field intensity image plot
```

Listing 3.20 MODE profiles for bent waveguides and calculations of mode-mismatch loss; bend_MODE.lsf

```
# bend_MODE.lsf: script to:
# 1) calculate the mode profile in a waveguide with varying bend radius
# 2) calculate mode mismatch loss with straight waveguide and radiation loss vs. radius

# Example with default parameters requires 1.2 GB ram.

radii= [0, 100, 50, 30, 20, 10, 5, 4, 3]*1e-6;
# min radius as defined in:
# http://docs.lumerical.com/en/solvers_finite_difference_eigenmode_bend.html
wg_2D_draw;  # run script to draw the waveguide

# define simulation parameters
wavelength   = 1.55e-6;
# maximum mesh size; 40 gives reasonable results
meshsize     = 10e-9;
modes        = 4;          # modes to output

# add 2D mode solver (waveguide cross-section)
addfde; set("solver type", "2D X normal");
set("x", 0);
width_margin = 2e-6; # ensure it is big enough to accurately measure radiation loss via
     PMLs
height_margin = 0.5e-6;
Zmin = -height_margin; Zmax = thick_Si + height_margin;
set('z max', Zmax); set('z min', Zmin);
Y_span = 2*width_margin + width_ridge;
Ymin = -Y_span/2; Ymax = -Ymin;
set('y',0); set('y span', Y_span);
set("wavelength", wavelength); set("solver type","2D X normal");
set("y min bc","PML"); set("y max bc","PML"); # radiation loss
set("z min bc","metal"); set("z max bc","metal"); # faster
set("define y mesh by","maximum mesh step");
set("dy", meshsize);
set("define z mesh by","maximum mesh step");
set("dz", meshsize);
set("number of trial modes",modes);
cleardcard; # Clears all the global d-cards.

# solve modes in the waveguide:
n=length(radii); Neff=matrix(n); LossdB_m=matrix(n);
LossPerBend=matrix(n); power_coupling=matrix(n);
for (i=1:n) {
  if (radii(i)==0) {
    setanalysis ('bent waveguide', 0); # Cartesian
  } else {
    setanalysis ('bent waveguide', 1); # cylindrical
    setanalysis ('bend radius', radii(i));
  }
  setanalysis ('number of trial modes', 4);
  nn = findmodes;
  if (nn>0) {
    Neff(i) = getdata('FDE::data::mode1','neff');
    LossdB_m(i) = getdata('FDE::data::mode1','loss'); # per m
    LossPerBend(i) = LossdB_m(i) * 2*pi*radii(i)/4;
    copydcard( 'mode1', 'radius' + num2str(radii(i)) );

    # Perform mode-overlap calculations between the straight and bent waveguides
    if (radii(i)>0) {
      out = overlap('::radius0','::radius'+num2str(radii(i)));
      power_coupling(i)=out(2); # power coupling
    }

    # plot mode profile:
    E3=pinch(getelectric('FDE::data::mode1')); y=getdata('FDE::data::mode1','y');
         z=getdata('FDE::data::mode1','z');
    image(y,z,E3);
    exportfigure('out/bend_mode_profile_radius'+ num2str(radii(i)));
```

```
    matlabsave('out/bend_mode_profile_radius'+ num2str(radii(i)), y,z,E3);
  }
}
PropagationLoss=2 *100; # dB/cm *100 --- dB/m
LossMM=-10*log10( power_coupling(2:n)^2 ); # plot 2X couplings per 90 degree bend vs
     radius (^2 for two)
LossR=LossPerBend (2:n)-LossPerBend(1);
LossP=PropagationLoss*2*pi*radii(2:n)/4; # quarter turn
plot ( radii (2:n)*1e6, LossMM, LossR, LossP, LossMM+LossR+LossP, "Radius [micron]", "Loss
     [dB]" ,"Bend Loss", "loglog, plot points");
legend ('Mode Mismatch Loss', 'Radiation loss','2 dB/cm propagation loss', 'Total Loss');
matlabsave ('out/bend_MODE_profiles_coupling', radii, power_coupling, LossPerBend);
```

References

[1] Dirk Taillaert, Harold Chong, Peter I. Borel, *et al.* "A compact two-dimensional grating coupler used as a polarization splitter". *IEEE Photonics Technology Letters* **15**.9 (2003), pp. 1249–1251 (cit. on p. 49).

[2] Dan-Xia Xu, J. H. Schmid, G. T. Reed, *et al*. "Silicon Photonic Integration Platform – Have We Found The Sweet Spot?". *IEEE Journal of Selected Topics in Quantum Electronics* **20**.4 (2014), pp. 1–17. ISSN: 1077-260X. DOI: 10.1109/JSTQE.2014.2299634 (cit. on p. 49).

[3] W. A. Zortman, D. C. Trotter, and M. R. Watts. "Silicon photonics manufacturing". *Optics Express* **18**.23 (2010), pp. 23598–23607 (cit. on p. 49).

[4] A. V. Krishnamoorthy, Xuezhe Zheng, Guoliang Li, *et al.* "Exploiting CMOS manufacturing to reduce tuning requirements for resonant optical devices". *IEEE Photonics Journal* **3**.3 (2011), pp. 567–579. DOI: 10.1109/JPHOT.2011.2140367 (cit. on p. 49).

[5] Edward Palik. *Handbook of Optical Constants of Solids.* Elsevier, 1998 (cit. on p. 50).

[6] Kurt Oughstun and Natalie Cartwright. "On the Lorentz–Lorenz formula and the Lorentz model of dielectric dispersion". *Optics Express* **11** (2003), pp. 1541–1546 (cit. on p. 50).

[7] Lorenzo Pavesi and Gérard Guillot. *Optical Interconnects: The Silicon Approach.* 978-3-540-28910-4. Springer Berlin/Heidelberg, 2006 (cit. on p. 50).

[8] G. Cocorullo and I. Rendina. "Thermo-optical modulation at 1.5 μm in silicon etalon". *Electronics Letters* **28**.1 (1992), pp. 83–85. DOI: 10.1049/el:19920051 (cit. on p. 51).

[9] J. A. McCaulley, V. M. Donnelly, M. Vernon, and I. Taha. "Temperature dependence of the near-infrared refractive index of silicon, gallium arsenide, and indium phosphide". *Physical Review B* **49**.11 (1994), p. 7408 (cit. on p. 51).

[10] Pieter Dumon. "Ultra-compact integrated optical filters in silicon-on-insulator by means of wafer-scale technology". PhD thesis. Gent University, 2007 (cit. on p. 51).

[11] Bradley J. Frey, Douglas B. Leviton, and Timothy J. Madison. "Temperature-dependent refractive index of silicon and germanium". *Proceedings SPIE.* Vol. 6273. 2006, 62732J–62732J–10. DOI: 10.1117/12.672850 (cit. on p. 51).

[12] Muzammil Iqbal, Martin A. Gleeson, Bradley Spaugh, *et al.* "Label-free biosensor arrays based on silicon ring resonators and high-speed optical scanning instrumentation". *IEEE Journal of Selected Topics in Quantum Electronics* **16**.3 (2010), pp. 654–661 (cit. on p. 52).

[13] Lukas Chrostowski, Samantha Grist, Jonas Flueckiger, *et al.* "Silicon photonic resonator sensors and devices". *Proceedings of SPIE Volume 8236; Laser Resonators, Microresonators, and Beam Control XIV* (Jan. 2012) (cit. on p. 52).

[14] Xu Wang, Samantha Grist, Jonas Flueckiger, Nicolas A. F. Jaeger, and Lukas Chrostowski. "Silicon photonic slot waveguide Bragg gratings and resonators". *Optics Express* **21** (2013), pp. 19 029–19 039 (cit. on p. 52).

[15] Xu Wang. "Silicon photonic waveguide Bragg gratings". PhD thesis. University of British Columbia, 2013 (cit. on p. 54).

[16] *Effective Mode Area – FDTD Solutions Knowledge Base.* [Accessed 2014/04/14]. URL: http://docs.lumerical.com/en/fdtd/user_guide_effective_mode_area.html (cit. on p. 61).

[17] A. Densmore, D. X. Xu, P. Waldron, *et al.* "A silicon-on-insulator photonic wire based evanescent field sensor". *IEEE Photonics Technology Letters* **18**.23 (2006), pp. 2520–2522 (cit. on p. 61).

[18] D. X. Xu, A. Delge, J. H. Schmid, *et al.* "Selecting the polarization in silicon photonic wire components". *Proceedings of SPIE.* Vol. 8266 (2012), 82660G (cit. on p. 61).

[19] N. Rouger, L. Chrostowski, and R. Vafaei. "Temperature effects on silicon-on-insulator (SOI) racetrack resonators: a coupled analytic and 2-D finite difference approach". *Journal of Lightwave Technology* **28**.9 (2010), pp. 1380–1391. DOI: 10.1109/JLT.2010.2041528 (cit. on p. 68).

[20] K. P. Yap, J. Lapointe, B. Lamontagne, *et al.* "SOI waveguide fabrication process development using star coupler scattering loss measurements". *Proceedings Device and Process Technologies for Microelectronics, MEMS, Photonics, and Nanotechnology IV, SPIE* (2008), p. 680014 (cit. on p. 69).

[21] Dietrich Marcuse. *Theory of Dielectric Optical Waveguides.* Elsevier, 1974 (cit. on p. 69).

[22] F. P. Payne and J. P. R. Lacey. "A theoretical analysis of scattering loss from planar optical waveguides". *Optical and Quantum Electronics* **26**.10 (1994), pp. 977–986 (cit. on p. 69).

[23] Christopher G. Poulton, Christian Koos, Masafumi Fujii, *et al.* "Radiation modes and roughness loss in high index-contrast waveguides". *IEEE Journal of Selected Topics in Quantum Electronics* **12**.6 (2006), pp. 1306–1321 (cit. on p. 69).

[24] Frdric Grillot, Laurent Vivien, Suzanne Laval, and Eric Cassan. "Propagation loss in single-mode ultrasmall square silicon-on-insulator optical waveguides". *Journal of Lightwave Technology* **24**.2 (2006), p. 891 (cit. on p. 69).

[25] Tom Baehr-Jones, Michael Hochberg, and Axel Scherer. "Photodetection in silicon beyond the band edge with surface states". *Optics Express* **16**.3 (2008), pp. 1659–1668 (cit. on p. 69).

[26] Jason J. Ackert, Abdullah S. Karar, John C. Cartledge, Paul E. Jessop, and Andrew P. Knights. "Monolithic silicon waveguide photodiode utilizing surface-state absorption and operating at 10 Gb/s". *Optics Express* **22**.9 (2014), pp. 10710–10715 (cit. on p. 69).

[27] A. D. Simard, N. Ayotte, Y. Painchaud, S. Bedard, and S. LaRochelle. "Impact of sidewall roughness on integrated Bragg gratings". *Journal of Lightwave Technology* **29**.24 (2011), pp. 3693–3704 (cit. on p. 69).

[28] Po Dong, Wei Qian, Shirong Liao, *et al.* "Low loss shallow-ridge silicon waveguides". *Optics Express* **18**.14 (2010), pp. 14 474–14 479 (cit. on p. 69).

[29] Yurii Vlasov and Sharee McNab. "Losses in single-mode silicon-on-insulator strip waveguides and bends". *Optics Express* **12**.8 (2004), pp. 1622–1631. DOI: 10.1364/OPEX.12.001622 (cit. on p. 70).

[30] Guoliang Li, Jin Yao, Hiren Thacker, *et al.* "Ultralow-loss, high-density SOI optical waveguide routing for macrochip interconnects". *Optics Express* **20**.11 (May 2012), pp. 12 035–12 039. DOI: 10.1364/OE.20.012035 (cit. on p. 70).

[31] Wim Bogaerts, Pieter Dumon, *et al.* "Compact wavelength-selective functions in silicon-on-insulator photonic wires". *IEEE Journal of Selected Topics in Quantum Electronics* **12**.6 (2006) (cit. on p. 70).

[32] Tom Baehr-Jones, Ran Ding, Ali Ayazi, *et al.* "A 25 Gb/s silicon photonics platform". *arXiv:1203.0767v1* (2012) (cit. on pp. 71, 72).

[33] *Using Mode Expansion Monitors – FDTD Solutions Knowledge Base.* [Accessed 2014/04/14]. URL: http://docs.lumerical.com/en/fdtd/user_guide_using_mode_expansion_monitors.html (cit. on p. 73).

[34] R. J. Bojko, J. Li, L. He, *et al.* "Electron beam lithography writing strategies for low loss, high confinement silicon optical waveguides". *Journal of Vacuum Science & Technology B: Microelectronics and Nanometer Structures* **29**.6 (2011), 06F309–06F309 (cit. on p. 73).

[35] *Bent Waveguide Calculation – MODE Solutions Knowledge Base.* [Accessed 2014/04/14]. URL: http://docs.lumerical.com/en/mode/usr_waveguide_bend.html (cit. on p. 75).

[36] Amnon Yariv and Pochi Yeh. *Photonics: Optical Electronics in Modern Communications (The Oxford Series in Electrical and Computer Engineering).* Oxford University Press, Inc., 2006 (cit. on pp. 77, 78).